

# Atlantic Climate Variability and Its Associated Atmospheric Circulation Cells

CHUNZAI WANG

*Physical Oceanography Division, Atlantic Oceanographic and Meteorological Laboratory, NOAA, Miami, Florida*

(Manuscript received 1 May 2001, in final form 19 October 2001)

## ABSTRACT

Phenomena important for Atlantic climate variability include the Atlantic zonal equatorial mode, the tropical Atlantic meridional gradient mode, and the North Atlantic Oscillation (NAO). These climate phenomena and their associated atmospheric circulation cells are described and discussed using the NCEP–NCAR reanalysis field and the NCEP sea surface temperature (SST) from January 1950 to December 1999. Atmospheric divergent wind and vertical motion are used for the identification of atmospheric circulation cells. During the peak phase of the Atlantic equatorial mode, the Atlantic Walker circulation weakens and extends eastward, which results in surface westerly wind anomalies in the equatorial western Atlantic. These westerly wind anomalies are partly responsible for warming in the equatorial eastern Atlantic that occurs in the second half of the year. The Atlantic equatorial mode involves a positive ocean–atmosphere feedback associated with the Atlantic Walker circulation, similar to the Pacific El Niño. The tropical Atlantic meridional gradient mode is characterized by a strong SST gradient between the tropical North Atlantic (TNA) and the tropical South Atlantic. Corresponding to the meridional gradient mode is an atmospheric meridional circulation cell in which the air rises over the warm SST anomaly region, flows toward the cold SST anomaly region aloft, sinks in the cold SST anomaly region, then crosses the equator toward the warm SST region in the lower troposphere. The analysis presented here suggests that the Pacific El Niño can affect the TNA through the Walker and Hadley circulations, favoring the TNA warming in the subsequent spring of the Pacific El Niño year. The NAO, characterized by strong westerly airflow between the Icelandic low and the Azores high, is also related to an atmospheric meridional circulation. During the high NAO index, the atmospheric Ferrel and Hadley cells are strengthened, consistent with surface westerly and easterly wind anomalies in the North Atlantic and in the mid-to-tropical Atlantic, respectively.

## 1. Introduction

Atlantic climate variability shows many important phenomena on different timescales. Similar to the tropical Pacific, the tropical Atlantic exhibits an equatorial cold tongue, and northeasterly and southeasterly trade winds converging into an intertropical convergence zone (ITCZ) north of the equator, all of which display a seasonal cycle. Unlike the tropical Pacific, the seasonal cycle dominates the ocean–atmosphere signal in the tropical Atlantic. Superimposed on the seasonal cycle is climate variability on interannual to interdecadal timescales. A phenomenon similar to but weaker than the Pacific El Niño also occurs in the Atlantic. The warm events reach their maximum strength in the second half of the year, with manifestations focused primarily near the equator (e.g., Zebiak 1993; Carton and Huang 1994; Latif and Grotzner 2000). During a warm phase, trade winds in the equatorial western Atlantic are weak and sea surface temperature (SST) is high in the equatorial eastern Atlantic. The converse occurs during a cold

phase. This interannual phenomenon is called the Atlantic zonal equatorial mode (or the Atlantic El Niño).

Early studies, using empirical orthogonal function (EOF) analysis or correlation of rainfall indices with SST fields, suggest that the tropical Atlantic also displays a “dipolelike” variation for SST, wherein the tropical regions to the north and south of the ITCZ are antisymmetric (e.g., Weare 1977; Hastenrath 1978; Moura and Shukla 1981; Servain 1991; Nobre and Shukla 1996). Recent modeling studies demonstrate the possibility that an ocean–atmosphere feedback mode may produce such antisymmetries on the decadal timescale (e.g., Chang et al. 1997; Xie 1999). The existence of such a dipole is controversial, however. For example, studies such as Houghton and Tourre (1992), Enfield and Mayer (1997), Mehta (1998), Enfield et al. (1999), and Dommenges and Latif (2000) suggest that the tropical North Atlantic (TNA) and tropical South Atlantic (TSA) SST anomalies occur independently and dipole configurations are not ubiquitous. Nevertheless, the index formed by the SST anomaly difference between the TNA and TSA (Servain 1991), sometimes referred to as a dipole index, has proved to be an invaluable indicator of the meridional gradient in SST anomaly that is correlated with north–south displacements of the

---

*Corresponding author address:* Dr. Chunzai Wang, NOAA/AOML/PhOD, 4301 Rickenbacker Causeway, Miami, FL 33149.  
E-mail: Chunzai.Wang@noaa.gov

ITCZ and with strong climate anomalies over the surrounding land regions. It thus can be more usefully regarded as a meridional gradient index. Moreover, much evidence exists for an ocean–atmosphere coupling—stronger in the TNA region—that causes reinforcement and persistence of meridional gradient anomalies through positive feedback involving the trade winds and associated surface flux anomalies (e.g., Carton et al. 1996; Chang et al. 1997; Xie 1999). This meridional antisymmetry appears to work preferentially at the decadal timescale (Mehta and Delworth 1995; Enfield et al. 1999), though it explains little of the total SST anomaly variance. In view of this and the possibly misleading nature of the term “dipole,” we prefer to refer to this variability simply as the tropical Atlantic meridional gradient mode.

Another important Atlantic climate phenomenon is the North Atlantic Oscillation (NAO) (e.g., Hurrell 1995, 1996) and its possible relationships and interactions with the tropical Atlantic. Much of the climate variability over the North Atlantic and surrounding continents has been correlated with changes in the intensity of the NAO. The NAO is associated with the variations of surface westerly wind in the midlatitude Atlantic, of the Icelandic low, and of the subtropical anticyclone centered near the Azores. Xie and Tanimoto (1998) suggested that extratropical variability drives tropical variability. Using an atmospheric general circulation model, Robertson et al. (2000) suggested an influence of the southern Tropics on the NAO. This may not be consistent, however, with the fact that the NAO index does not significantly relate to the TSA SST anomalies. Deque and Servain (1989) emphasized the importance of the atmospheric circulation over the North Atlantic midlatitudes in tropical Atlantic SST. Ruiz-Barrades et al. (2000) recently concluded that the extratropical Atlantic does not affect the tropical Atlantic, but that there are some impacts of the Tropics on the extratropics.

As summarized above, all of these Atlantic climate phenomena have been previously studied through either data analyses or numerical models. However, variations of the atmospheric Walker, Hadley, and Ferrel circulation cells associated with these Atlantic climate phenomena have not been documented and they have been little studied. The recent availability of the National Centers for Environmental Prediction–National Center for Atmospheric Research (NCEP–NCAR) reanalysis fields provides a good opportunity to investigate the atmospheric circulation cells. The present paper analyzes the Atlantic Walker, Hadley, and Ferrel cells associated with Atlantic climate phenomena, using recent available oceanic and atmospheric data. It also discusses possible linkages and mechanisms of these Atlantic climate phenomena. The rest of the paper is organized as follows. Section 2 introduces the data used in this paper. Section 3 shows the annual variability of the atmospheric circulation patterns associated with the Atlantic Walker, Hadley, and Ferrel cells. Sections 4, 5, 6, and

7 document atmospheric circulation cells associated with the Atlantic zonal equatorial mode, the tropical Atlantic meridional gradient mode, the remote influence of the Pacific El Niño on the TNA, and the NAO, respectively. Section 8 provides a discussion and summary.

## 2. Data

The major data source in this study is the NCEP–NCAR reanalysis fields from January 1950 to December 1999. The NCEP–NCAR reanalysis fields use a state-of-the-art global data assimilation system on a  $2.5^\circ$  longitude by  $2.5^\circ$  latitude grid [see Kalnay et al. (1996) for details]. Variables used in this study are monthly sea level pressure (SLP) and monthly atmospheric horizontal wind velocity, vertical velocity, and velocity potential at levels of 1000, 925, 850, 700, 600, 500, 400, 300, 250, 200, 150, and 100 mb. The vertical component of wind field in the reanalysis fields is pressure vertical velocity. In our presentation, we multiply the pressure vertical velocity by  $-1$ , so positive values of the vertical velocity indicate an upward movement of air parcels. Since we are interested in tropical atmospheric circulation and northern midlatitude atmospheric circulation associated with Atlantic climate variability, our analyses in this paper are shown from  $30^\circ\text{S}$  to  $75^\circ\text{N}$  over the Atlantic and the eastern Pacific. Note that our analyses were performed globally and results associated with Pacific ENSO are reported in a companion paper (Wang 2002).

Horizontal wind velocity can be divided into a non-divergent (or rotational) part and a divergent (or irrotational) part (e.g., Mancuso 1967; Krishnamurti 1971; Krishnamurti et al. 1973):  $\mathbf{v} = \mathbf{v}_\psi + \mathbf{v}_\phi = \mathbf{k} \times \nabla\psi + \nabla\phi$ , where  $\psi$  is streamfunction and  $\phi$  is velocity potential. The first part does not contribute to atmospheric divergent fields associated with atmospheric vertical motion (it is nondivergent). It is well known that the Walker and Hadley cells are thermally driven, associated with atmospheric convergence–divergence. Atmospheric heating associated with convection induces atmospheric convergence–divergence that drives atmospheric vertical motion and circulation. What matters to atmospheric cells associated with atmospheric convergence–divergence is the divergent part of the wind, although the rotational part is usually larger. Therefore, atmospheric divergent wind and vertical motion are used for the identification of atmospheric circulation cells (Hastenrath 2001).

Monthly SST data are also used in this study. SST data are taken from the NCEP SST dataset on a  $2^\circ$  latitude by  $2^\circ$  longitude grid from January 1950 to December 1999. These SST fields were produced by using a spatial interpolation method employing EOF analysis [see Smith et al. (1996) for the detailed description]. With all of these data, we first calculate monthly climatologies based on the full record period (1950–99)

and then anomalies are obtained by subtracting the monthly climatologies for each dataset from the individual monthly data.

### 3. Annual variability

To better understand anomaly variations of atmospheric circulation cells associated with Atlantic climate variability, we first examine annual variability of tropospheric circulation patterns. Figure 1 shows the boreal winter (January) climatologies of tropospheric circulation. Centers of low (high) velocity potential are associated with divergent outflow (convergent inflow) winds. Figures 1a–c show that divergence (convergence) in the upper troposphere corresponds to convergence (divergence) in the lower troposphere, and is associated with upward (downward) vertical motion in the midtroposphere (three levels of 200, 500, and 850 mb, are chosen as representative of the upper, mid-, and lower troposphere, respectively). Centers of upper-tropospheric divergence and lower-tropospheric convergence over the Amazon and tropical Africa are characterized by midtropospheric upward motions. These patterns are consistent with three of the known major global heat sources over: the Amazon, tropical Africa, and the Maritime Continent of the western Pacific [the western Pacific maritime continent heat source associated with Pacific ENSO is described in the companion paper of Wang (2002)]. The tropical South and North Atlantic is associated with upper-tropospheric convergence, lower-tropospheric divergence, and midtropospheric downward vertical motion. The extratropical North Atlantic also shows a strong ascending motion. Figure 1d shows the east–west circulation cell near the equator—the Atlantic zonal Walker cell. The air ascends in the west, diverges eastward aloft, sinks in the east, and returns toward the west. However, the sinking and westward flows do not reach the lower troposphere during the boreal winter.

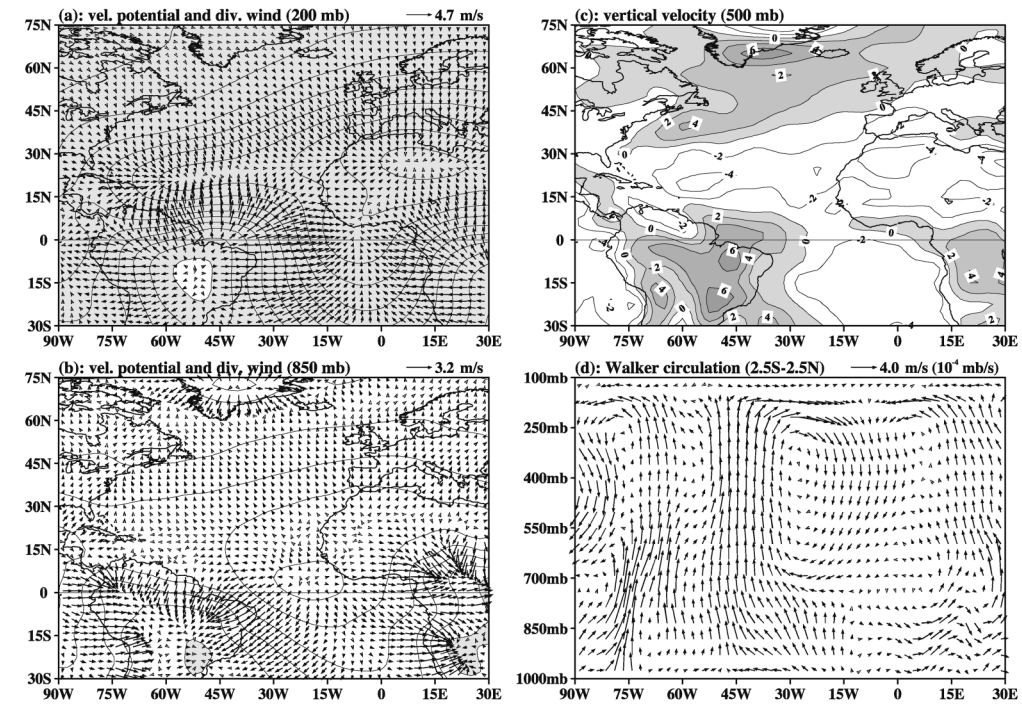
As suggested by Figs. 1a–c, the meridional circulation in the western Atlantic is different from that in the eastern Atlantic. Thus, we separately plot meridional–vertical circulations in the west (60°–40°W) and in the east (10°W–10°E) as shown in Figs. 1e–h. In the west, the meridional circulation has two cells: the Hadley cell and the Ferrel cell. The Hadley cell comprises air rising over south America, then diverging northward in the upper troposphere, descending over the northern subtropical Atlantic, and flowing southward across the equator to the Southern Hemisphere (SH) in the lower troposphere (Fig. 1e). The Ferrel cell has upward motion in the mid- and high latitudes, and downward motion in the northern subtropical Atlantic. In the east, the tropical meridional circulation cells are shallow (constrained to the lower troposphere) during the boreal winter (Fig. 1g). Air rises around 10°N, diverges northward and southward near 700 mb, descends in the north and south subtropical Atlantic, and then returns to the surface convergent re-

gion. However, the Ferrel cell shows a deep-tropospheric circulation during the boreal winter. The zonal wind shows a core of maximum westerly wind (jet stream) just below the tropopause around 200 mb in both the west and east (Figs. 1f and 1h). The jet stream in the east is more intense and is closer to the equator. The lower troposphere in both the east and the west shows easterly winds in the Tropics and westerly winds in the midlatitude. In the east, the lower troposphere also displays westerly winds near the surface just north of the equator.

The boreal summer (July) climatologies of tropospheric circulation are shown in Fig. 2. The centers of upper-tropospheric divergence and lower-tropospheric convergence associated with midtropospheric ascent shift to the Northern Hemisphere (NH). For example, the ascent over the Amazon (during the boreal winter) now shifts to the Intra-Americas Sea (IAS). This is associated with variability of the tropical Western Hemisphere warm pool (WHWP) that extends from the eastern North Pacific to the Gulf of Mexico, the Caribbean, and the western tropical North Atlantic (Wang and Enfield 2001). As showed and discussed by Wang and Enfield (2001), the WHWP is dominated by SSTs in excess of 28.5°C at that time, associated with eastern North Pacific and Atlantic hurricane activities, and rainfall from northern South America to the southern tier of the United States. Consistent with these northward shifts, the Atlantic Walker circulation (Fig. 2d) shows a weaker upward motion and a stronger downward motion (compared to the boreal winter) in the west and east, respectively. The strong midtropospheric ascent of the boreal winter in the North Atlantic now disappears (Fig. 2c).

Associated with the northward shifts during the boreal summer, the Hadley circulation in the west also shows a northward shift, with a strong upward vertical motion near the equator. The Hadley circulation in the west has double cells: one in the tropical NH and the other one in the tropical SH. In the east, the Hadley circulation cell now becomes a deep tropospheric circulation. Both the east and the west show cross-equatorial flows from the SH to the NH in the lower troposphere. During that time, the NH jet stream weakens and moves northward. The reason for weakening and northward movement of the jet stream is due to the change of the atmospheric temperature gradient (Holton 1992). The pole-to-equator temperature gradient in NH troposphere is much larger in the boreal winter than in the boreal summer. Since the zonal wind and temperature fields satisfy the thermal wind relationship to a high degree of accuracy, the maximum zonal wind speed in the NH is much larger in the boreal winter than in the boreal summer. Figure 2f also shows a low-level easterly jet located at about 700 mb over the western subtropical Atlantic around 15°N. Westerly wind of the eastern Atlantic near the surface north of the equator is further developed during

**Climatologies (January)**



**Climatologies (January)**

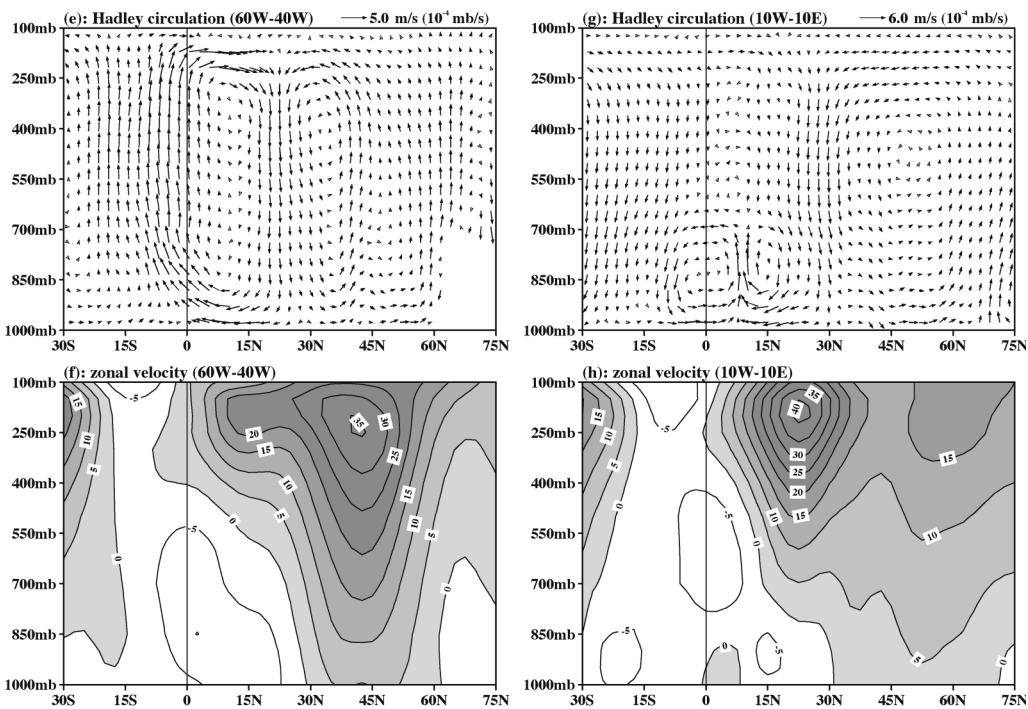
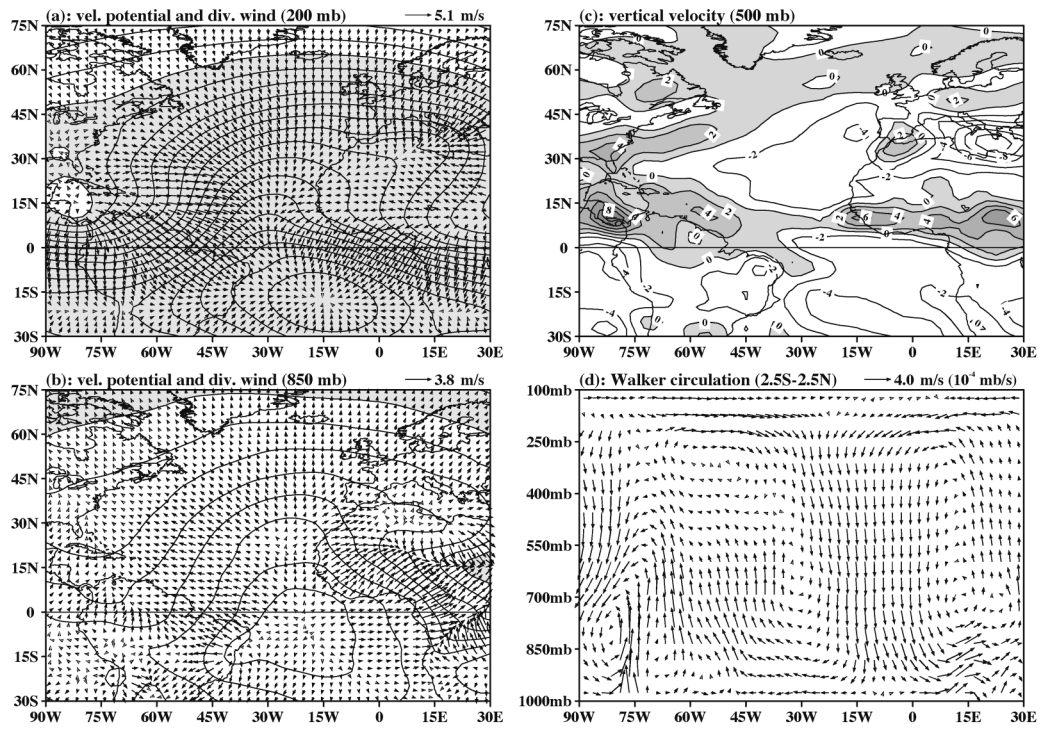


FIG. 1. The boreal winter (Jan) climatologies of tropospheric circulation patterns. (a) 200-mb velocity potential ( $10^6 \text{ m}^2 \text{ s}^{-1}$ ) and divergent wind ( $\text{m s}^{-1}$ ), (b) 850-mb velocity potential ( $10^6 \text{ m}^2 \text{ s}^{-1}$ ) and divergent wind ( $\text{m s}^{-1}$ ), (c) 500-mb vertical velocity ( $10^{-4} \text{ mb s}^{-1}$ ), (d) zonal-vertical circulation cross section by averaging divergent wind and vertical velocity between  $2.5^\circ\text{S}$  and  $2.5^\circ\text{N}$ , (e) meridional-vertical circulation cross section in the west by averaging divergent wind and vertical velocity between  $60^\circ$  and  $40^\circ\text{W}$ , (f) zonal wind cross section in the west between  $60^\circ$  and  $40^\circ\text{W}$ , (g) meridional-vertical circulation cross section in the east by averaging divergent wind and vertical velocity between  $10^\circ\text{W}$  and  $10^\circ\text{E}$ , (h) zonal wind cross section in the east between  $10^\circ\text{W}$  and  $10^\circ\text{E}$ . The vertical velocity is taken to be the negative of the pressure vertical velocity in the reanalysis; i.e., positive values indicate an upward movement of air parcels. Positive values are shaded.

Climatologies (July)



Climatologies (July)

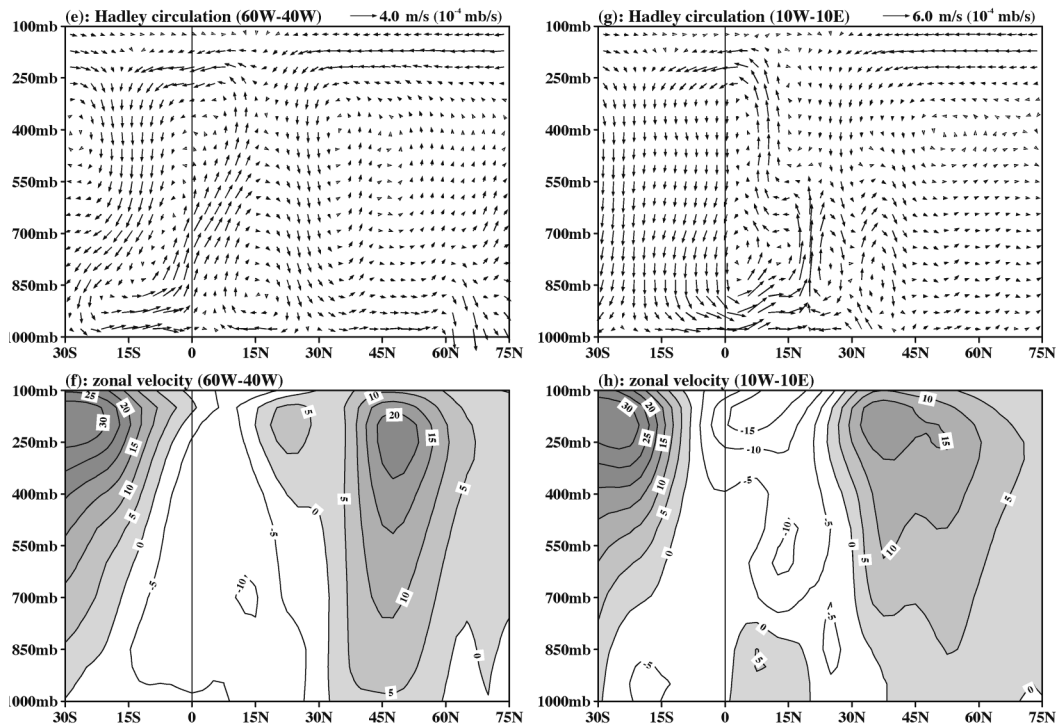


FIG. 2. As in Fig. 1, but for the boreal summer (Jul).

### Atlantic Equatorial Mode and Pacific El Niño

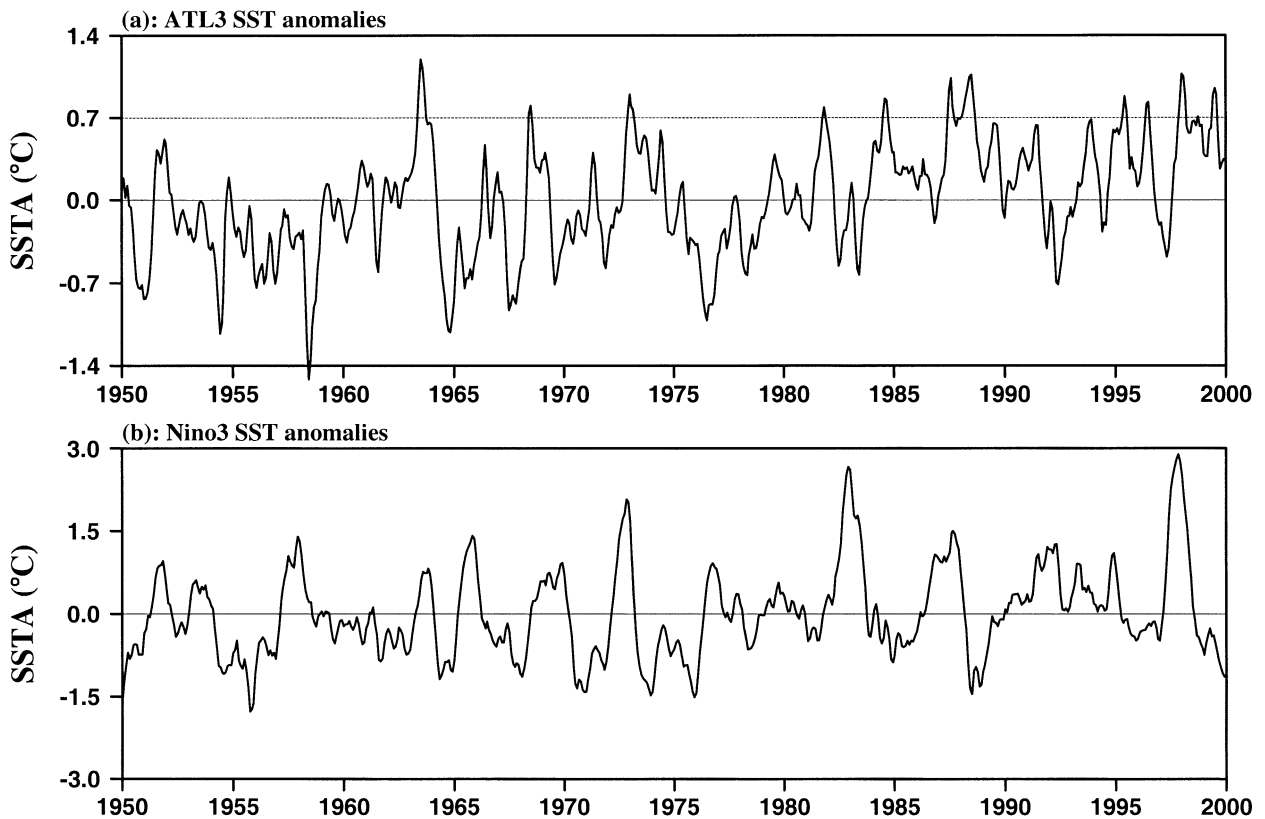


FIG. 3. Three-month running means of (a) SST anomalies in the ATL3 region ( $3^{\circ}\text{S}$ – $3^{\circ}\text{N}$ ,  $20^{\circ}\text{W}$ – $0^{\circ}$ ) and (b) SST anomalies in the Niño-3 region ( $5^{\circ}\text{S}$ – $5^{\circ}\text{N}$ ,  $150^{\circ}$ – $90^{\circ}\text{W}$ ). The straight dashed line in (a) represents SST anomalies of  $0.7^{\circ}\text{C}$ .

the boreal summer (Fig. 2h), associated with the African monsoon.

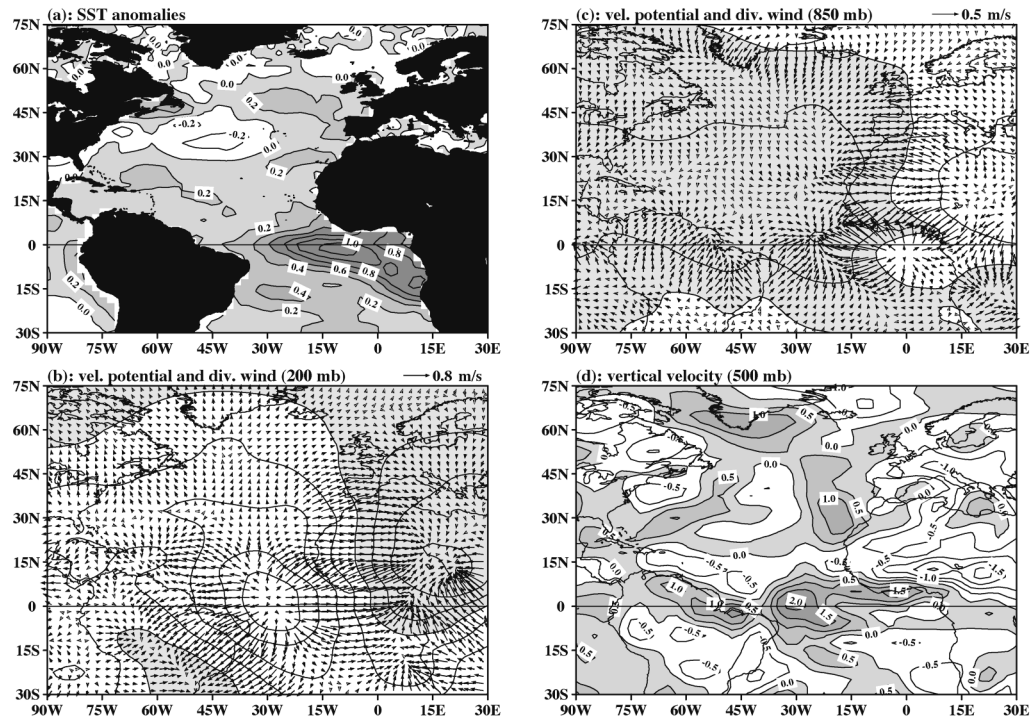
#### 4. The Atlantic zonal equatorial mode

As discussed in Zebiak (1993), Carton and Huang (1994), and Latif and Grotzner (2000), an interannual phenomenon similar to but weaker than the Pacific El Niño also occurs in the Atlantic. The largest near-equatorial SST anomalies occur in the equatorial eastern Atlantic. Figure 3 shows the SST anomalies in (Fig. 3a) the ATL3 region ( $3^{\circ}\text{S}$ – $3^{\circ}\text{N}$ ,  $20^{\circ}\text{W}$ – $0^{\circ}$ ) and (Fig. 3b) in the Niño-3 region ( $5^{\circ}\text{S}$ – $5^{\circ}\text{N}$ ,  $150^{\circ}$ – $90^{\circ}\text{W}$ ). Despite smaller amplitude, the ATL3-SST anomalies also show an interannual oscillation. During the 50-yr period since 1950 there are 11 significant warm events in which the ATL3 SST anomalies exceed  $0.7^{\circ}\text{C}$  and last more than 1 month. The maximum ATL3 SST anomalies in Fig. 3a for these warm events are centered in July 1963, July 1968, January 1973, November 1981, August 1984, August 1987, July 1988, June 1995, July 1996, January 1998, and July 1999. Among these 11 warm events, the peak phase of the ATL3-SST anomalies occurs in the boreal summer for 8 events and in the boreal winter for 3 events. Thus, the Atlantic equatorial mode also seems

to be phase-locked to the seasonal cycle. Notice that the mature phase of the Pacific El Niño warm events occurs in the boreal winter except for the 1986–87 event that has double peaks with the major one in the boreal summer.

We calculated the lagged cross correlation between the ATL3 and Niño-3 SST anomalies. The maximum negative correlation of  $-0.15$  and positive correlation of  $0.26$  occur when the ATL3 SST anomalies lead and lag the Niño-3 SST anomalies by 9 and 18 months, respectively. However, these values are below the 99% significance level of  $0.32$ . Notice that in all of our correlation calculations, degrees of freedom are determined by the integral timescale after Sciremammano (1979). The low correlation suggests that local ocean–atmosphere coupling may play a role in the variations of the Atlantic equatorial mode. Zebiak (1993) showed that the interactions between the tropical Atlantic Ocean and atmosphere can produce an interannual oscillation similar to the Pacific El Niño mode, despite a non-self-sustaining feature (a damped oscillation). Delecluse et al. (1994) and Latif and Grotzner (2000) emphasized the remote influence of the Pacific El Niño on the Atlantic equatorial mode. It is possible that both the local

## Atlantic Equatorial Mode



## Atlantic Equatorial Mode

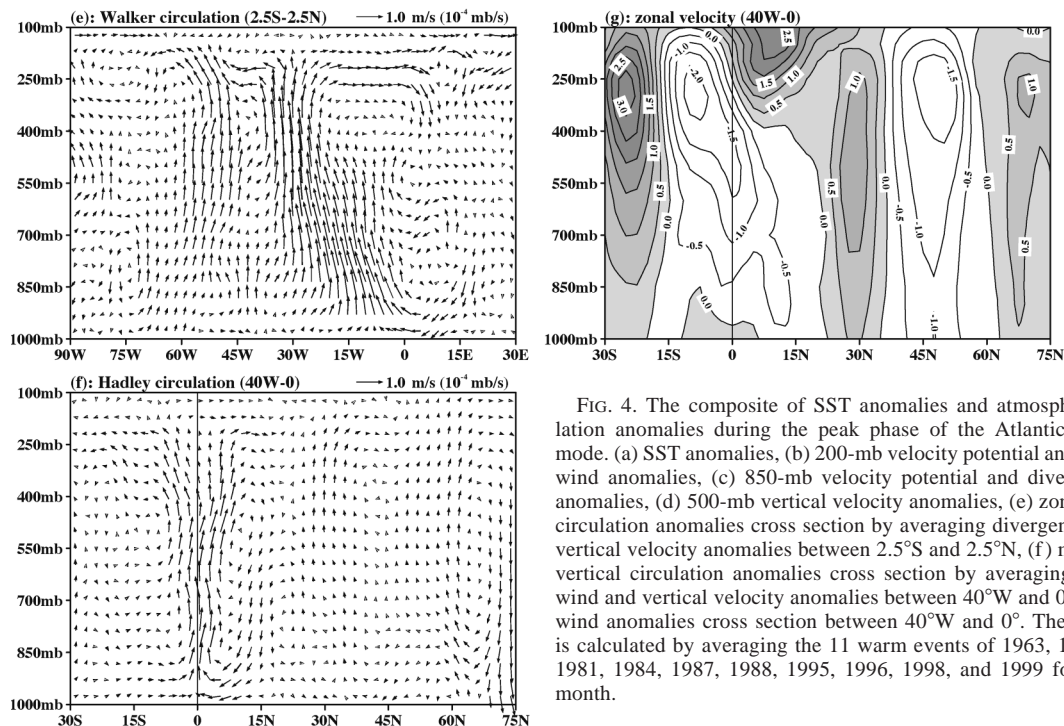


FIG. 4. The composite of SST anomalies and atmospheric circulation anomalies during the peak phase of the Atlantic equatorial mode. (a) SST anomalies, (b) 200-mb velocity potential and divergent wind anomalies, (c) 850-mb velocity potential and divergent wind anomalies, (d) 500-mb vertical velocity anomalies, (e) zonal-vertical circulation anomalies cross section by averaging divergent wind and vertical velocity anomalies between 2.5°S and 2.5°N, (f) meridional-vertical circulation anomalies cross section by averaging divergent wind and vertical velocity anomalies between 40°W and 0°, (g) zonal wind anomalies cross section between 40°W and 0°. The composite is calculated by averaging the 11 warm events of 1963, 1968, 1973, 1981, 1984, 1987, 1988, 1995, 1996, 1998, and 1999 for the peak month.

coupling and the remote forcing contribute to the Atlantic equatorial mode.

Three-dimensional atmospheric circulation patterns associated with the Atlantic equatorial mode can be seen

by compositing the 11 warm events mentioned above. Figure 4 shows the distribution of SST anomalies and atmospheric circulation anomalies during the peak phase of the Atlantic equatorial mode. The entire tropical and

subtropical Atlantic show positive SST anomalies, with maximum SST anomalies confined to the equatorial eastern Atlantic. Negative and positive SST anomalies appear in the central mid-Atlantic and in the northeast Atlantic, respectively. The upper-tropospheric anomalous divergent outflow in the tropical western Atlantic corresponds to the lower-tropospheric anomalous convergent inflow, whereas the equatorial eastern Atlantic, specifically, the Gulf of Guinea, and the eastern tropical Africa land region show the upper-tropospheric anomalous convergent inflow and lower-tropospheric anomalous divergent outflow. Associated with these anomalous divergent–convergent flow fields are midtropospheric anomalous ascending motion near the region of the equatorial Atlantic, anomalous descending motion in the subtropical Atlantic (along 15°N), and anomalous ascending motion in the North Atlantic (north of 25°N). The equatorial zonal circulation shows anomalous ascending motion in the equatorial western Atlantic (Fig. 4e). Although Fig. 4e does not seem to show a clear anomalous zonal cell, we know that the Atlantic Walker cell is weakened and extended eastward during the peak phase of the Atlantic equatorial mode if we consider the mean state of the Atlantic Walker cell in Fig. 2d. The anomalous Hadley circulation shows ascent near the equator and descent in the subtropical region near 15°N. The zonal wind in Fig. 4g shows that the equatorial troposphere above 850 mb has zonal easterly wind anomalies, whereas the surface exhibits zonal westerly wind anomalies. This is similar to the wind distribution during the mature phase of the Pacific El Niño. The troposphere also shows westerly wind anomalies centered around 70°N, 30°N, and 25°S and easterly wind anomalies around 45°N and 10°S.

To see whether or not these atmospheric circulation patterns are evident in every warm event over the period of record, we plot the time series for evolution of the Atlantic equatorial mode. Based on the composites in Fig. 4, we calculate and plot in Fig. 5 the following time series: (Fig. 5a) 1000-mb zonal wind anomalies in the region of 2.5°S–2.5°N, 40°–20°W (the ATL4 region) for measuring the zonal wind variations, (Fig. 5b) 500-mb vertical velocity anomalies in the region of 2.5°S–2.5°N, 40°–20°W for measuring the Atlantic Walker circulation, and (Fig. 5c) 500-mb vertical velocity anomaly difference between the regions of 12.5°–17.5°N, 40°W–0° and 2.5°S–2.5°N, 40°W–0° for measuring the Hadley circulation. These time series are compared with the ATL3 SST anomalies, as shown in Fig. 5. When the equatorial eastern Atlantic is warm, westerly wind anomalies usually appear in the equatorial western Atlantic. The correlation calculation (in Fig. 5a) shows that the maximum correlation of 0.28 (which is below the 95% significance level) occurs when the ATL3 SST anomalies lag the ATL4 zonal wind anomalies by one month. Thus, the ATL3 SST anomalies do not highly and significantly correlate with the ATL4 zonal wind anomalies. Again, this suggests that the Atlantic equatorial mode may be forced both locally and remotely.

Both the Atlantic Walker and Hadley circulations show high correlations (in Fig. 5b,c) with the ATL3 SST anomalies (–0.66 and 0.67, respectively). Thus, corresponding to the Atlantic equatorial mode is a weakening of the Atlantic Walker circulation and a strengthening of the Atlantic Hadley circulation.

## 5. The tropical Atlantic meridional gradient mode

Many studies have defined indices for measuring the tropical Atlantic meridional gradient mode (e.g., Servain 1991; Rajagopalan et al. 1998; Xie and Tanimoto 1998; Enfield et al. 1999). We define a tropical North Atlantic (TNA) index (5°–25°N, 55°–15°W) and a tropical South Atlantic (TSA) index (0°–20°S, 30°W–10°E) to measure SST anomaly variations in the tropical NH and SH, respectively. In Fig. 6a, the time series of the TNA and TSA SST anomalies are shown and in Fig. 6b the SST anomaly difference between the TNA and TSA regions is shown. The calculation of cross correlation shows that the TNA SST anomalies do not significantly correlate with the TSA SST anomalies at any time lags, in agreement with Rajagopalan et al. (1998) and Enfield et al. (1999). However, about half the time either TSA or TNA (but not the other) may be anomalous, while 12%–15% of the time they may be both anomalous and of opposite sign (Enfield et al. 1999). Thus, under most circumstances, even in the absence of anticorrelation, the anomalous meridional gradient of SST is likely nonzero and can be associated with atmospheric climate departures (e.g., Moura and Shukla 1981; Folland et al. 1986; Nobre and Shukla 1996). The SST anomaly difference between the TNA and TSA regions is thus defined to measure the meridional gradient mode. Figure 6b shows that the main feature of the interhemispheric SST gradient is a slow variation on a decadal timescale. The meridional SST gradient is mainly positive for the periods of pre-1970, 1976–83, and after-1990 but prevailing negative during 1971–75 and 1984–89.

The structure of SST anomalies and atmospheric circulation anomalies for the meridional gradient mode can be seen by calculating the anomaly difference between a positive phase and a negative phase. Figure 7 shows the anomaly difference between the period of 1966–70 and the period of 1971–75. The tropical Atlantic SST anomalies show opposite sign: the TNA is warm and the TSA is cold, with the TNA being stronger than the TSA. The mid-Atlantic along the east coast of the United States and the North Atlantic show cold and warm SST anomalies, respectively. The upper (lower) troposphere shows anomalous convergent inflow (divergent outflow) in the equatorial region and anomalous divergent outflow (convergent inflow) in the TNA and midlatitude (Figs. 7b and 7c). Correspondingly, the midtroposphere is associated with anomalous descending motion in the TSA and over the Amazon, anomalous ascending mo-

## Atlantic Equatorial Mode

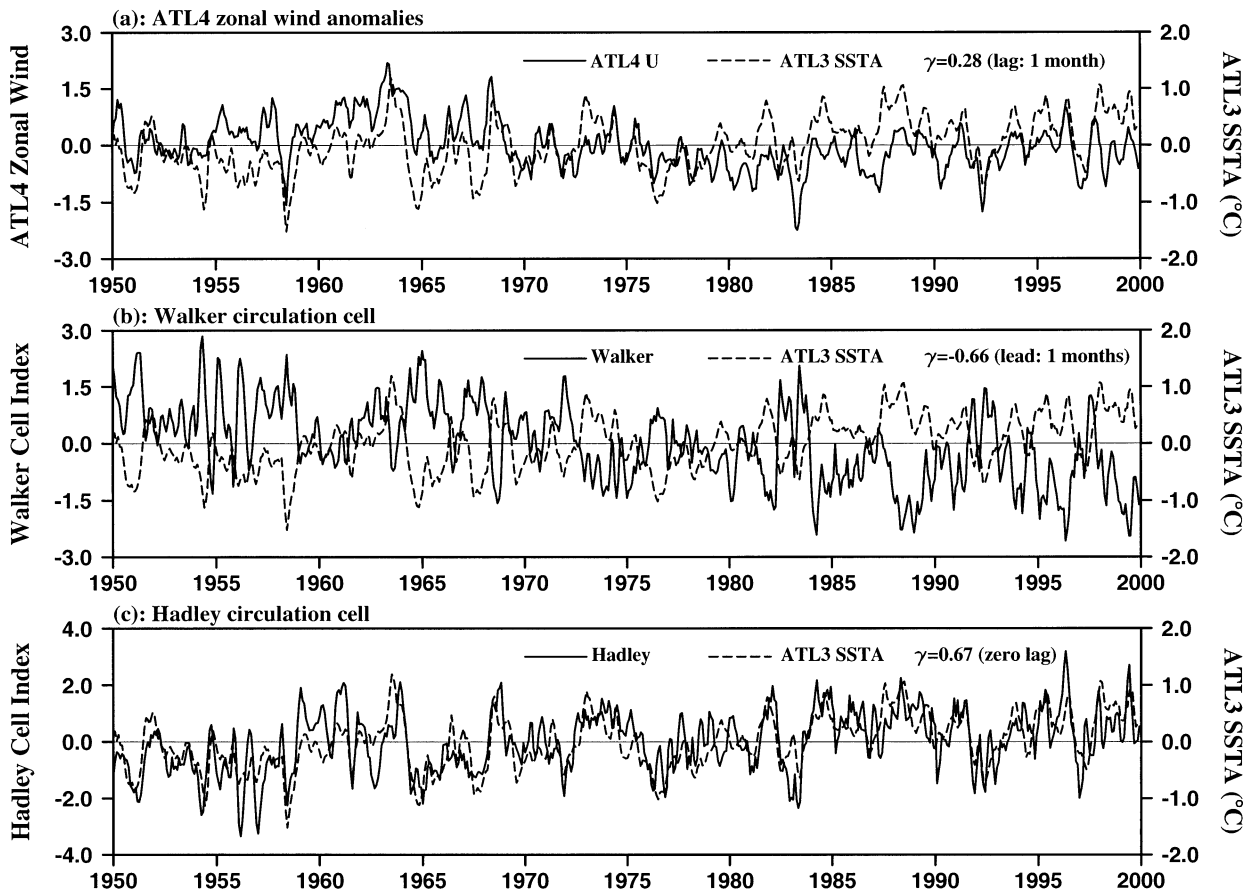


FIG. 5. Comparisons of the ATL3-SSTA anomalies with (a) 1000-mb zonal wind anomalies in the ATL4 region ( $2.5^{\circ}\text{S}$ – $2.5^{\circ}\text{N}$ ,  $40^{\circ}$ – $20^{\circ}\text{W}$ ), (b) the Atlantic Walker circulation cell index, and (c) the Atlantic Hadley circulation cell index. The Atlantic Walker cell index is defined by 500-mb vertical velocity anomalies in the region of  $2.5^{\circ}\text{S}$ – $2.5^{\circ}\text{N}$ ,  $40^{\circ}$ – $20^{\circ}\text{W}$ . The Atlantic Hadley cell index is defined by 500-mb vertical velocity anomaly difference between the regions of  $12.5^{\circ}$ – $17.5^{\circ}\text{N}$ ,  $40^{\circ}\text{W}$ – $0^{\circ}$  and  $2.5^{\circ}\text{S}$ – $2.5^{\circ}\text{N}$ ,  $40^{\circ}\text{W}$ – $0^{\circ}$ . All of the time series are 3-month running means. The  $\gamma$  represents the correlation coefficient.

tion in the TNA and in the midlatitude, and anomalous descending motion in the North Atlantic (Fig. 7d). The meridional anomalous circulation shows that the air rises over the TNA warm waters, diverges southward and northward aloft, converges in the upper troposphere to feed the strong subsidence and lower-tropospheric divergence in the equatorial TSA, then crosses the equator toward the TNA in the lower troposphere (Fig. 7e). This meridional cell is northern; that is, it corresponds more closely to the NH Hadley circulation. The zonal wind in the lower troposphere shows easterly anomalies in the southern TSA and westerly wind anomalies in the TNA and near the equatorial region (Fig. 7f), consistent with trade wind weakening (strengthening) in the TNA (TSA). The upper-troposphere wind shows an alternating pattern of positive–negative zonal wind anomalies near  $15^{\circ}\text{S}$ ,  $15^{\circ}\text{N}$ ,  $30^{\circ}\text{N}$ , and  $60^{\circ}\text{N}$ .

The time series of the zonal wind anomalies and the Hadley circulation cell associated with the meridional gradient mode are shown in Figs. 8a and 8b, respec-

tively. The zonal wind anomalies associated with the meridional gradient mode are plotted by subtracting 1000-mb zonal wind anomalies in the TSA region from those in the TNA region, and the Hadley circulation is measured by 500-mb vertical velocity anomaly difference between the regions of  $2.5^{\circ}$ – $7.5^{\circ}\text{S}$ ,  $40^{\circ}$ – $20^{\circ}\text{W}$  and  $25^{\circ}$ – $30^{\circ}\text{N}$ ,  $40^{\circ}$ – $20^{\circ}\text{W}$ . The maximum correlations of the zonal wind anomaly difference and the Hadley circulation with the meridional SSTA gradient are 0.67 and 0.59, respectively when the meridional SSTA gradient mode lags the zonal wind anomaly difference and the Hadley circulation by two and one months, respectively. Thus, the tropical Atlantic meridional gradient mode is associated with the variations of the NH Hadley circulation and of the zonal wind in the TNA and TSA.

## 6. The remote influence of the Pacific El Niño on the TNA

Previous studies have shown that the TNA SSTA anomalies are related to the Pacific El Niño (e.g., Curtis and

## Meridional Gradient Mode

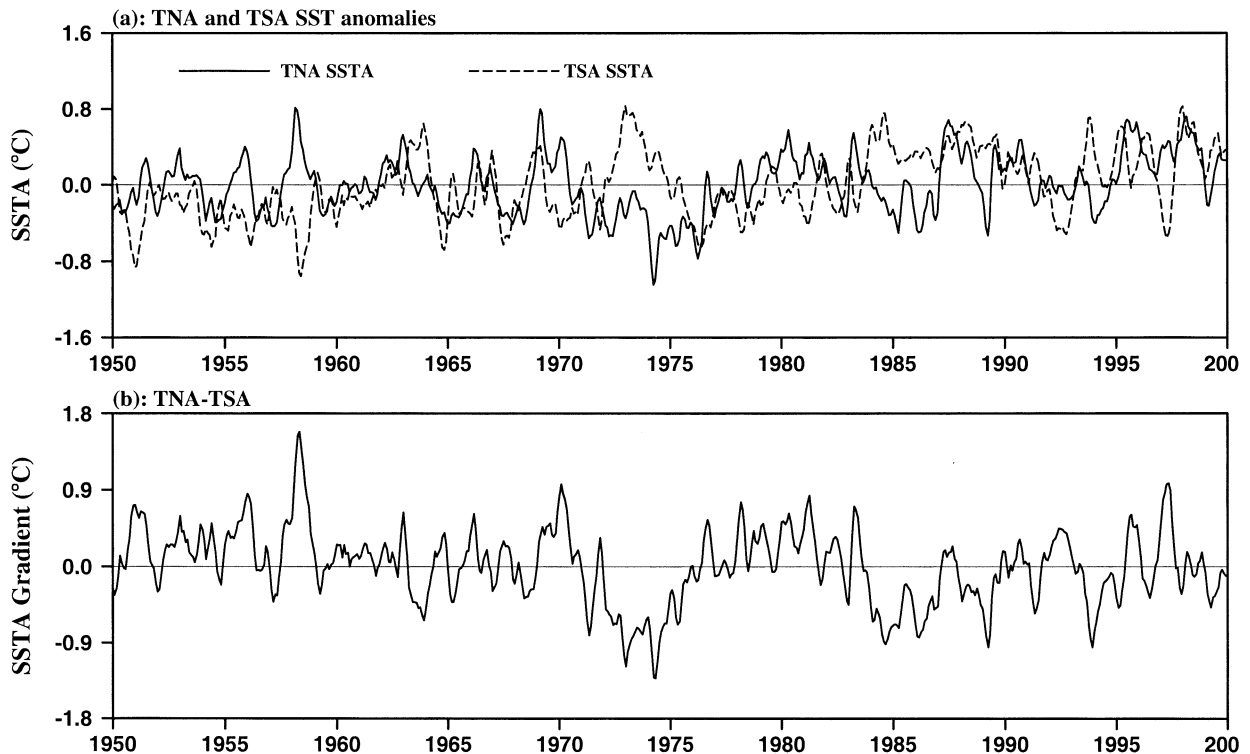


FIG. 6. Three-month running means of (a) SST anomalies in the TNA region ( $5^{\circ}$ – $25^{\circ}$ N,  $55^{\circ}$ – $15^{\circ}$ W) and SST anomalies in the TSA region ( $0^{\circ}$ – $20^{\circ}$ S,  $30^{\circ}$ W– $10^{\circ}$ E), and (b) SST anomaly difference between the TNA and TSA.

Hastenrath 1995; Enfield and Mayer 1997; Klein et al. 1999; Hastenrath 2000). We calculate the lagged cross correlation between the TNA and Niño-3 SST anomalies. The maximum positive correlation of 0.47 occurs when the TNA SST anomalies lag the Niño-3 SST anomalies by five months. (Correlation between the TSA and Niño-3 SST anomalies shows that the TSA does not significantly correlate with the Pacific El Niño.) Since the mature phase of the Pacific El Niño occurs around December of the Pacific El Niño year, the TNA SST anomalies thus tend to peak in the subsequent May of the Pacific El Niño year. Curtis and Hastenrath (1995) and Enfield and Mayer (1997) have suggested that the Pacific El Niño affects TNA northeast trade winds that reduce latent heat flux and then increase the TNA SST, consistent with Figs. 7a and 7f. The questions are how the Pacific El Niño affects the TNA trade winds and why the TNA warming occurs five months later, rather than in the mature phase of the Pacific El Niño. Next, we consider the remote influence of the Pacific El Niño on the TNA SST anomalies from a Walker and Hadley circulation point of view.

We compute composites of the midtropospheric vertical velocity and the upper-tropospheric divergent wind field in the tropical eastern Pacific and Atlantic. The composite calculation is based on the criteria in which the Niño-3 SST anomalies exceed  $1^{\circ}$ C and the subse-

quent TNA warming is larger than  $0.5^{\circ}$ C. The 1957/58, 1982/83, and 1997/98 El Niño events and their associated subsequent TNA warmings satisfy these criteria, and they are used to calculate the composites. Figure 9 shows the composites during the mature phase of the Pacific El Niño (December) and the subsequent spring (May). During the mature phase of the Pacific El Niño, the centers of upper-tropospheric anomalous divergent outflow are located in the equatorial eastern Pacific and the southeast of the United States, and the center of upper-tropospheric anomalous convergent inflow is over South America and TNA (Fig. 9b). Accompanied with the upper-tropospheric anomalous divergent outflow (convergent inflow) is midtropospheric anomalous ascending (descending) motion (Fig. 9a). The strong anomalous ascent and subsidence are over the regions of the northern Atlantic subtropical high and the TNA, respectively. These patterns do not favor SST warming during that time, but lead to the TNA warming in the subsequent spring. During the subsequent months, the Pacific El Niño begins to decay as evidenced by a decrease in the anomalous ascending motion and divergent wind anomalies in the equatorial eastern Pacific. However, anomalous ascending motion and divergent wind in the far equatorial eastern Pacific are intensified (Figs. 9c and 9d). This anomalous intensification results in a change in atmospheric cells over the tropical Atlantic.

## Meridional Gradient Mode

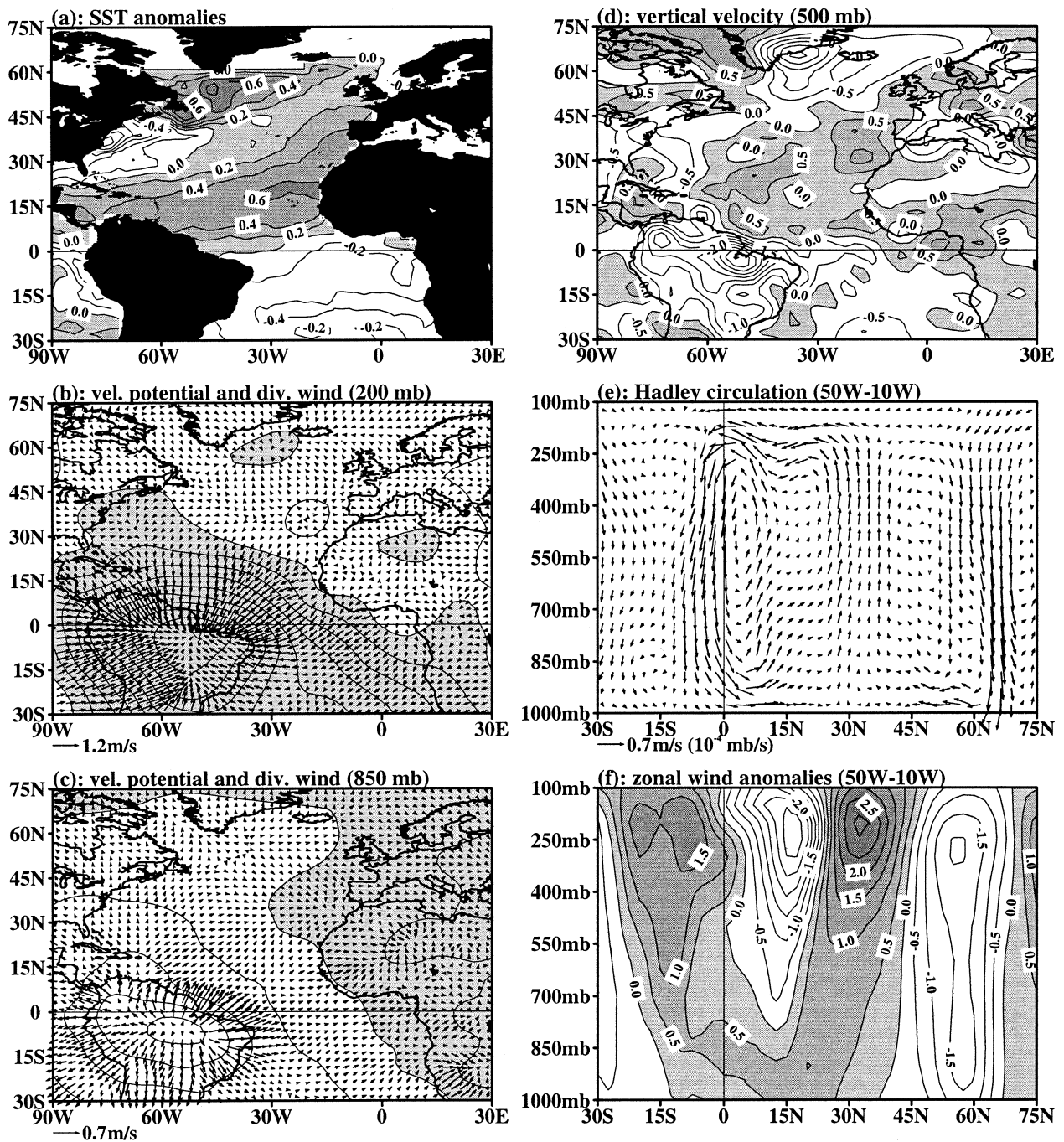


FIG. 7. The structures of SST anomalies and atmospheric circulation anomalies for the meridional gradient mode. (a) SST anomalies, (b) 200-mb velocity potential and divergent wind anomalies, (c) 850-mb velocity potential and divergent wind anomalies, (d) 500-mb vertical velocity anomalies, (e) meridional-vertical circulation anomalies cross section by averaging divergent wind and vertical velocity anomalies between 50° and 10°W, (f) zonal wind anomalies cross section between 50° and 10°W. The structures are calculated by the anomaly difference between the positive phase period of 1966–70 and the negative phase period of 1971–75.

The anomalous Walker and Hadley cells over the tropical Atlantic in the subsequent May of the Pacific El Niño year are shown in Figs. 10a and 10b, respectively. The air anomalously ascends in the far equatorial eastern

Pacific, diverges eastward and westward in the upper troposphere, and then descends over the equatorial Atlantic (Fig. 10a). Associated with this anomalous Atlantic Walker circulation is an anomalous Hadley cir-

## Meridional Gradient Mode

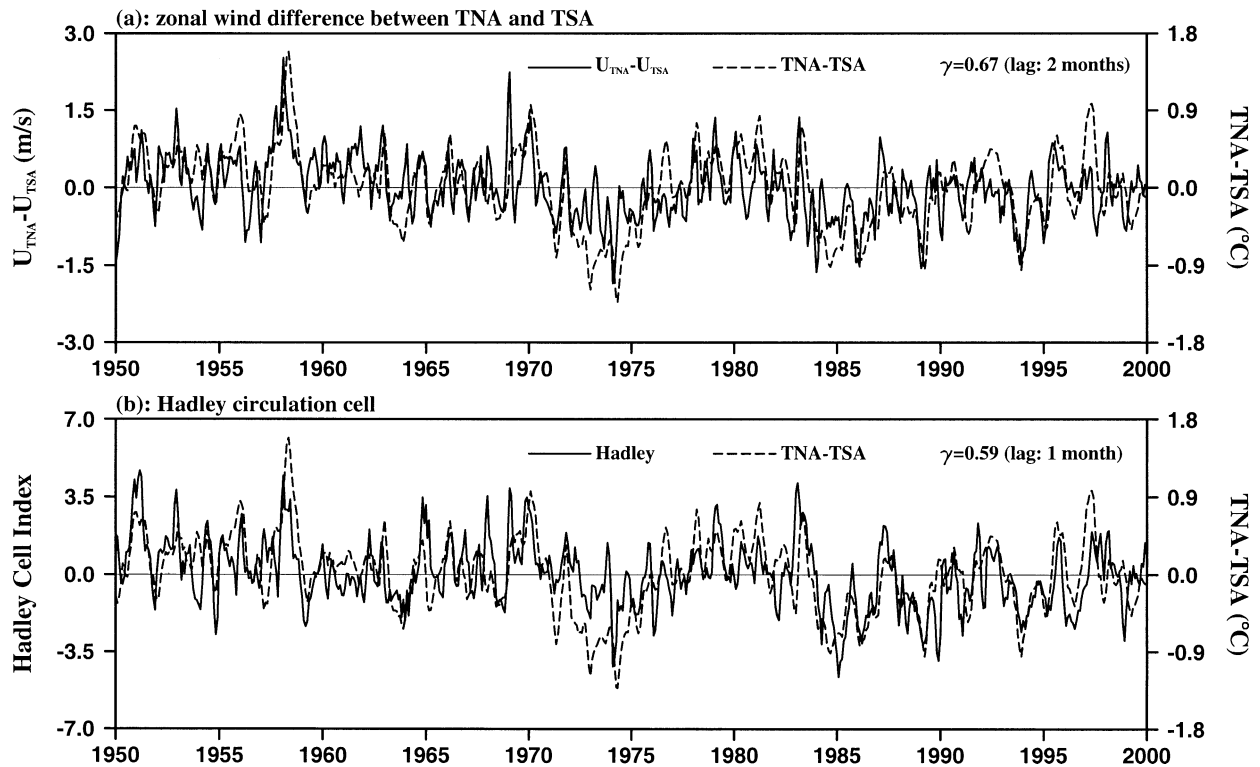


FIG. 8. Comparisons of the tropical Atlantic meridional SST gradient with (a) the zonal wind anomaly difference between the TNA and TSA, (b) the Hadley circulation cell index. The Hadley cell index is defined by the 500-mb vertical velocity anomaly difference between the regions of  $2.5^{\circ}$ – $7.5^{\circ}$ S,  $40^{\circ}$ – $20^{\circ}$ W, and  $25^{\circ}$ – $30^{\circ}$ N,  $40^{\circ}$ – $20^{\circ}$ W. All of the time series are 3-month running means. The  $\gamma$  represents correlation coefficient.

ulation cell in the Atlantic (Fig. 10b). The Hadley cell shows an anomalous subsidence over the equatorial Atlantic and the TSA. The air crosses the equator and flows from the TSA to the TNA in the lower troposphere. The TNA is thus associated with a strong anomalous ascending motion as shown in Fig. 10b. The TNA ascent is associated with low SLP anomalies that push the subtropical anticyclone northward and decrease the northeast trade winds and latent heat flux (e.g., Curtis and Hastenrath 1995; Enfield and Mayer 1997), and then increases the TNA SST anomalies during that time. The connection between the Pacific El Niño and the TNA during the subsequent spring of the Pacific El Niño year, observed from the NCEP–NCAR reanalysis fields, is schematically summarized in Fig. 11. Further discussions of the TNA warming [including possible effect of the Pacific–North American (PNA) pattern] are given in section 8.

## 7. The North Atlantic Oscillation

Another important climate phenomenon in the Atlantic is the NAO whose positive phase is characterized by strong westerly airflow between the Icelandic low and the Azores high, particularly in winter. Hurrell (1995,

1996) defined a NAO index as the difference of winter (December–March) SLP anomalies between Lisbon, Portugal ( $38.43^{\circ}$ N,  $9.08^{\circ}$ W), and Stykkisholmur, Iceland ( $65.06^{\circ}$ N,  $22.48^{\circ}$ W). Figure 12 shows the NAO index calculated from the NCEP–NCAR reanalysis fields. A striking feature of the NAO index has been the reversal from the weak meridional SLP gradient to predominantly positive index values starting near 1970. The winters of 1972/73, 1982/83, 1988/89, 1989/90, 1992/93, and 1994/95 are marked by high positive values of the NAO index.

The structures of SST and atmospheric variables for the high NAO index can be calculated by compositing anomalies of the 1972/73, 1982/83, 1988/89, 1989/90, 1992/93, and 1994/95 winters. Figure 13 shows the composites of (a) SST and (b) SLP anomalies. The Atlantic shows an alternating pattern of zonally oriented positive–negative SST anomalies. The coolings appear in the North Atlantic and in the TNA. The warmings occur in the mid-Atlantic with centers located at the east coast of the United States and the west coast of Europe, and in the TSA. As shown later (Fig. 16c), the TSA SST anomalies do not significantly correlate with the NAO index [also see the regression figure of Visbeck et al. (1998)]. Thus, in spite of seemingly being a quad-

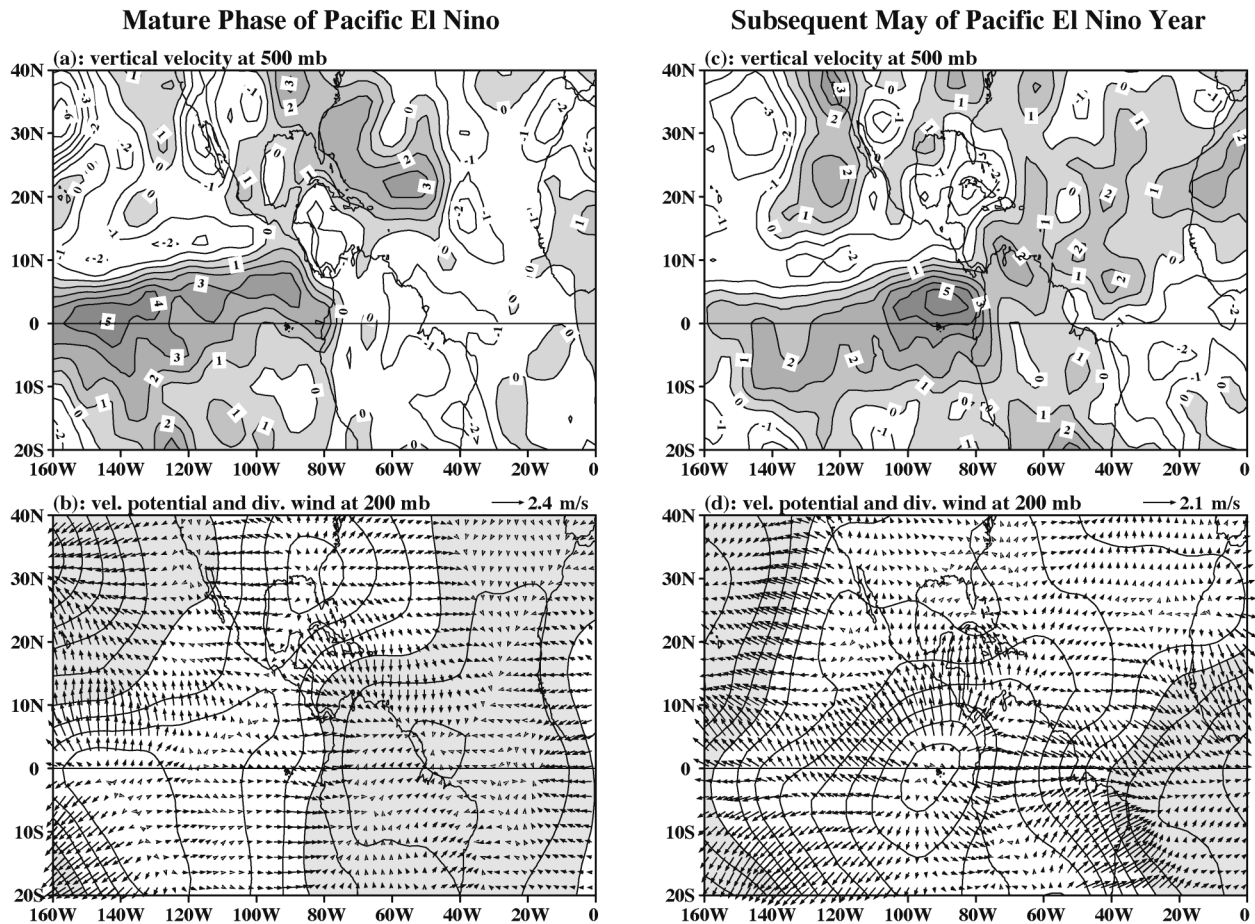


FIG. 9. Atmospheric circulation patterns during the mature phase of the Pacific El Niño (left) and subsequent May of the Pacific El Niño year (right). (a) 500-mb vertical velocity anomalies averaged over Dec of 1957, 1982, and 1997. (b) 200-mb velocity potential and divergent wind anomalies averaged over Dec of 1957, 1982, and 1997. (c) 500-mb vertical velocity anomalies averaged over May of 1958, 1983, and 1998. (d) 200-mb velocity potential and divergent wind anomalies averaged over May of 1958, 1983, and 1998.

riple pattern, the spatial Atlantic SST pattern of the NAO is a tripole (e.g., Rodwell et al. 1999; Seager et al. 2000). The SLP anomalies simply show a meridional seesaw pattern, with low SLP anomalies in the North Atlantic and high SLP anomalies south of about 55°N.

During the high NAO index, upper-tropospheric anomalous divergent outflow centers are over the Amazon and the North Atlantic, whereas an upper-tropospheric anomalous convergent inflow center is located in northern Africa and Europe (Fig. 14a). Corresponding to these upper-tropospheric anomalous divergent and convergent centers are the respective lower-tropospheric anomalous convergent and divergent flows. The mid-troposphere shows anomalous ascending motion in the North Atlantic and over the Amazon, and anomalous descending motion in the central to eastern mid-Atlantic (Fig. 14c). Note that Europe and Africa also show anomalous descending motion. The anomalous meridional circulation shows a counterclockwise circulation cell in the North Atlantic and a clockwise cell in the tropical mid-Atlantic (Fig. 14d). These two cells correspond to

the Ferrel cell and the Hadley cell, respectively. These anomalous cells have the same rotations as the mean Ferrel and Hadley cells, indicating that during the high NAO index, both the Ferrel cell and the Hadley cell are strengthened. Zonal wind anomalies display westerly wind anomalies in the North Atlantic and easterly wind anomalies in the subtropical Atlantic (Fig. 14e), consistent with the strength of the Icelandic low and the Azores high during the high NAO index. These wind anomaly patterns extend throughout the whole troposphere, with the maximum zonal wind anomalies occurring in the upper troposphere. The distribution of the wind patterns seems to suggest that wind speed associated with latent heat flux is responsible for the SST anomaly patterns shown in Fig. 13a (we will discuss this issue in detail in the next section).

The change of the wind and atmospheric circulation cells associated with the NAO can be further seen from the time series. Based on Fig. 14, we choose 1000-mb zonal wind anomalies in the region of 50°–60°N, 30°W–0° for the surface westerly wind change; 1000-mb zonal

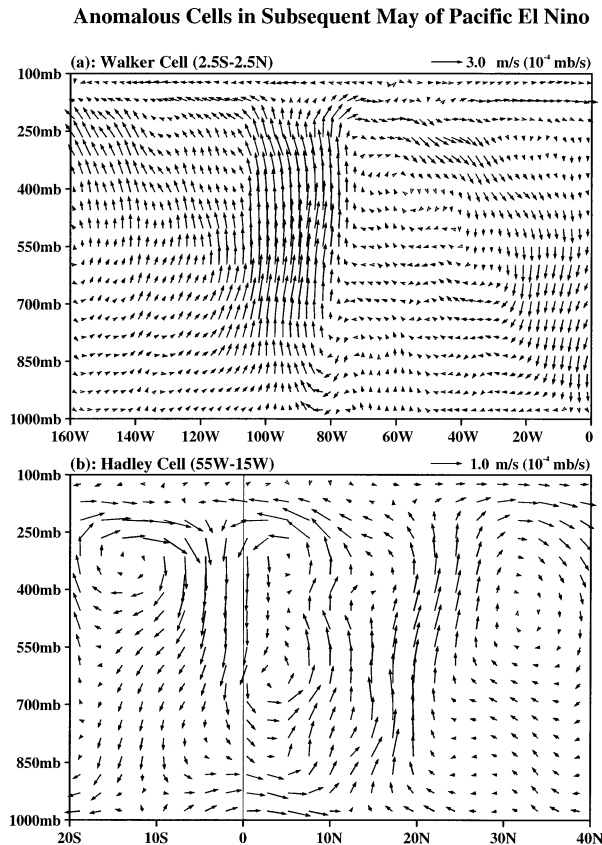


FIG. 10. The anomalous (a) Walker and (b) Hadley circulation cells in the subsequent May of the Pacific El Niño year. The Walker cell is plotted by averaging divergent wind and vertical velocity anomalies between 2.5°S and 2.5°N over May of 1958, 1983, and 1998. The Hadley cell is plotted by averaging divergent wind and vertical velocity anomalies between 55° and 15°W over May of 1958, 1983, and 1998.

wind anomalies in the region of 25°–35°N, 30°W–0° for the surface easterly wind change; 500-mb vertical velocity anomaly difference between the regions of 35°–40°N, 30°W–0° and 60°–65°N, 30°W–0° for the Ferrel cell; and 500-mb vertical velocity anomaly difference between the regions of 35°–40°N, 30°W–0° and 15°–20°N, 30°W–0° for the Hadley cell. These time series are compared with the NAO index, and shown in Figs. 15a–d. All of these indices are highly correlated with the NAO index. Every NAO event is associated with westerly wind anomalies between the Icelandic low and the Azores high and easterly wind anomalies south of the Azores high. Both the Ferrel cell and the Hadley cell are also closely related to the NAO index, suggesting that the meridional circulation cells may be important for the NAO.

## 8. Discussion and summary

There are three major localized tropical heat sources: one migrates between the Amazon and the IAS; one is

over tropical Africa; and the largest one is over the Maritime Continent, which comprises Indonesia, Malaysia, the surrounding islands, and adjacent oceanic regions. It is widely known that zonal excursion of the Maritime Continent heat source is associated with the Pacific ENSO phenomenon. The present paper discusses the heat sources of the IAS–Amazon and tropical Africa and their associated Atlantic climate variability. The heat sources move seasonally, generally, being most north and west in the boreal summer, and south and east in the boreal winter. For example, the heat source of the IAS–Amazon is centered over the Amazon in the boreal winter, whereas it migrates to the IAS in the boreal summer. Associated with the seasonal movements of the heat sources are the seasonal variations of the atmospheric meridional Hadley cell and Ferrel cell, and Atlantic Walker cell. The NH jet stream is strong and southernmost in the boreal winter, whereas it weakens and moves northward during the boreal summer.

Interannual east–west motion of the Pacific Walker circulation, associated with large changes in atmospheric convection, plays an important role in the evolution of the Pacific El Niño (e.g., Philander 1990; Neelin et al. 1998). We found a similar relationship between the Atlantic Walker circulation cell and the Atlantic equatorial mode. During the warm phase of the Atlantic equatorial mode, ascending motion associated with the IAS–Amazon heat source extends eastward. This eastward extension weakens the Atlantic Walker circulation cell and thus decreases surface equatorial easterly wind in the western Atlantic, which increases SST in the equatorial eastern Atlantic. Thus, the positive ocean–atmosphere interaction associated with the Pacific Walker cell, being responsible for the Pacific El Niño, is also operating in the Atlantic. However, since the IAS–Amazon heat source is primarily over land and the basin size of the tropical Atlantic is smaller, the positive feedback associated with the Atlantic Walker circulation is not as strong as that in the Pacific. This may explain why the Atlantic equatorial mode is weak and the coupled ocean–atmosphere mode of Zebiak (1993) is a damped oscillation. In fact, this is also consistent with the fact of the low correlation between the ATL3 SST and ATL4 zonal wind anomalies. In addition to local coupling, the remote forcing may also play a role in the Atlantic equatorial mode (e.g., Servain et al. 1982; Latif and Grotzner 2000). For example, the Pacific El Niño may force the Atlantic equatorial mode (e.g., Delecluse et al. 1994). During the warm phase of Pacific ENSO, easterly wind anomalies prevail over the equatorial Atlantic. These depress (raise) the thermocline in the equatorial western (eastern) Atlantic. The equatorial Atlantic will adjust slowly to these low-frequency wind variations and the western equatorial signal will propagate slowly eastward, thus warming will appear later in the equatorial eastern Atlantic. In nature, both local and remote effects are responsible for the Atlantic equatorial mode. Since none of these effects is dominant, the ATL3

### Connection of Pacific ENSO with the Tropical North Atlantic (TNA)

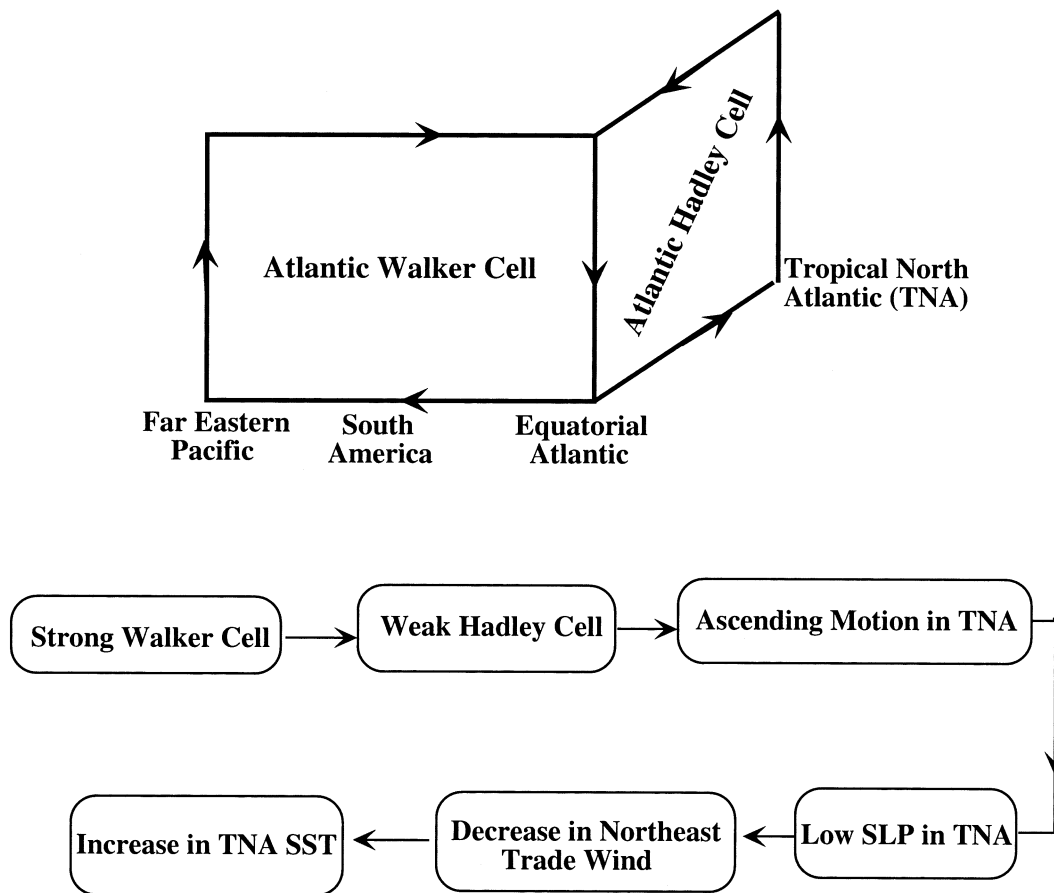


FIG. 11. Schematic diagram showing how the Pacific El Niño affects the TNA SST anomalies. The anomalous Walker and Hadley cells are drawn, based on the data presented in Fig. 10.

SST anomalies are not well correlated with either of the ATL4 zonal wind anomalies and Niño-3 SST anomalies.

The Atlantic is unique in having the tropical meridional gradient mode. The meridional gradient mode is characterized by when the TNA is anomalous or when the TSA is anomalous, or when both conditions exist nearly simultaneously and are opposite in sign. Corresponding to this meridional mode is an atmospheric meridional circulation cell in which the air rises over the warm SST anomaly region, flows toward the cold SST anomaly region aloft, converges in the upper troposphere to feed the strong subsidence and lower-tropospheric divergence in the cold SST anomaly region, then crosses the equator toward the warm SST anomaly region in the lower troposphere. Since the lower-tropospheric air always crosses the equator toward the warm SST anomalies, the Coriolis force will deflect air to the east (the west) over the warm (cold) SST anomaly regions. Tropical zonal wind anomalies are westerly (east-

erly) over the warm (cold) anomaly regions in the lower troposphere. These anomaly winds will decrease (increase) wind speed in the warm (cold) anomaly regions that, in turn, decreases (increases) latent heat flux (e.g., Curtis and Hastenrath 1995; Enfield and Mayer 1997) and thus results in further increase (decrease) of SST in the warm (cold) SST anomaly region.

The TNA SST warming occurs about five months after the mature phase of the Pacific El Niño. There are two possible ways for the Pacific El Niño to affect the TNA SST anomalies: 1) through the PNA pattern; 2) through the Walker and Hadley circulations. Wallace and Gutzler (1981) and Horel and Wallace (1981) found that equatorial Pacific warming is accompanied by a teleconnection PNA pattern that shows alternating positive and negative geopotential height anomalies emanated from the Pacific, directed poleward, curved eastward, and then equatorward. It is possible that the Pacific El Niño affects the northern Atlantic subtropical

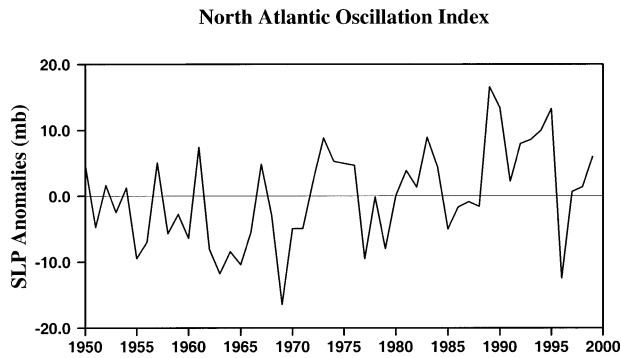


FIG. 12. The NAO index calculated by the difference of winter (Dec–Mar) SLP anomalies between Lisbon, Portugal (38.43°N, 9.08°W), and Stykkisholmur, Iceland (65.06°N, 22.48°W).

high through the PNA pattern. Changes of the Atlantic subtropical high induce variations of the northeast trade winds on its southern flank and then affect the TNA SST anomalies. Our analysis in this paper focuses on the Walker and Hadley circulations for linking the Pacific El Niño and the TNA. During the mature phase of the Pacific El Niño, the TNA is associated with anomalous descending motion and anomalous ascending motion is located in the region of the northern Atlantic subtropical high. However, during the subsequent months, when the Pacific El Niño begins to decay, the Atlantic Walker and meridional Hadley circulation cells are stronger and weaker, respectively. The atmospheric circulation cell change results in anomalous ascending motion in the TNA that decreases SLP and pushes the subtropical anticyclone northward, then decreases the northeast trade winds and latent heat flux, and thus increases the TNA SST anomalies.

We have discussed the relationships of the ATL3, TNA, and TSA SST anomalies with the Pacific El Niño; however, we have not addressed relationships among the Atlantic modes. First, we consider relationship between the Atlantic equatorial mode and the tropical Atlantic meridional gradient mode. The lagged cross correlation between the ATL3 SST anomalies and the meridional SST gradient shows a maximum negative correlation of  $-0.55$  at zero time lag (not shown), suggesting that there may be a possible linkage between the Atlantic equatorial mode and the meridional gradient mode (Servain et al. 1999, 2000; Sutton et al. 2000). In order to investigate possible relations of the NAO with other modes, we calculate the winter (December–March) indices of Niño-3, ATL3, TSA, TNA, and TNA minus TSA. The resulting time series are compared with the NAO index, as shown in Fig. 16. The Pacific decadal oscillation (PDO) is evident in the winter Niño-3 index (Mestas-Núñez and Enfield 2001). The warming phase of the PDO occurred around 1976. The timing of the reversal to a strongly positive NAO index since the 1970s seems to be coincident with the climate shift in the PDO. The positive NAO index since the 1970s is

### High NAO Index

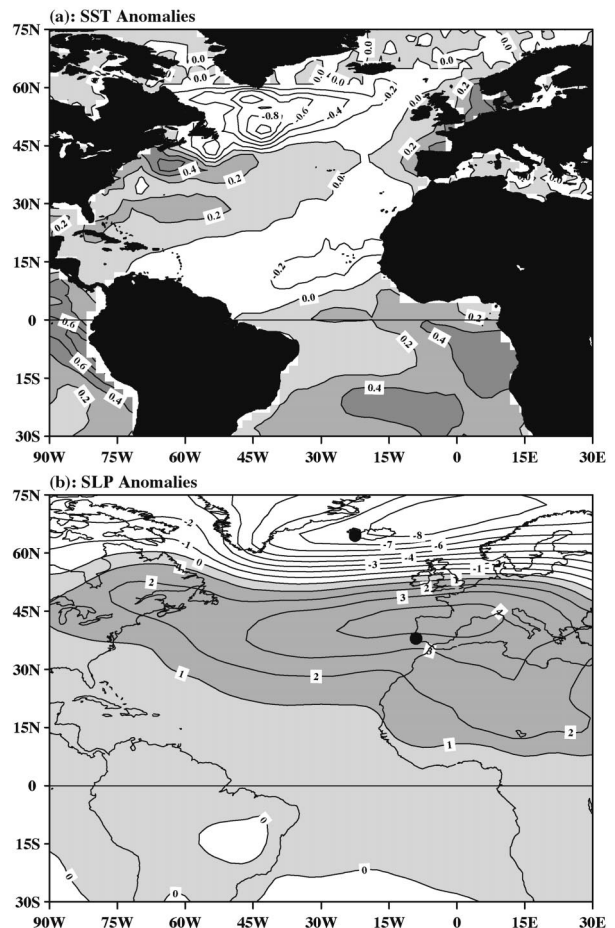


FIG. 13. The structures of (a) SST anomalies and (b) SLP anomalies for the high NAO indices of the 1972/73, 1982/83, 1988/89, 1989/90, 1992/93, and 1994/95 winters. The two dots in (b) are Lisbon, Portugal (38.43°N, 9.08°W) and Stykkisholmur, Iceland (65.06°N, 22.48°W), which are used to calculate the NAO index.

also associated with positive winter ATL3 and TSA SST anomalies. However, our calculations show that the correlation coefficients of the NAO index with the Niño-3, ATL3, and TSA indices are 0.09, 0.26, and 0.25, respectively, all of which are below the 95% significance levels. Thus, the NAO seems not to significantly relate to the Pacific El Niño, the Atlantic El Niño, and the TSA on interannual timescales. Our calculations also show that the correlation coefficients of the NAO index with the TNA and TNA minus TSA indices are  $-0.33$  and  $-0.41$ , respectively, which are both above the 95% significance levels. The NAO is significantly correlated with and is out of phase with the TNA and the tropical Atlantic meridional gradient mode. Recently, Rajagopalan et al. (1998) and Robertson et al. (2000) suggested possible interactions between the NAO and the tropical and subtropical Atlantic. However, our calculations do not show a significant relation between the NAO and the TSA, consistent with the result of Visbeck et al.

## High NAO Index

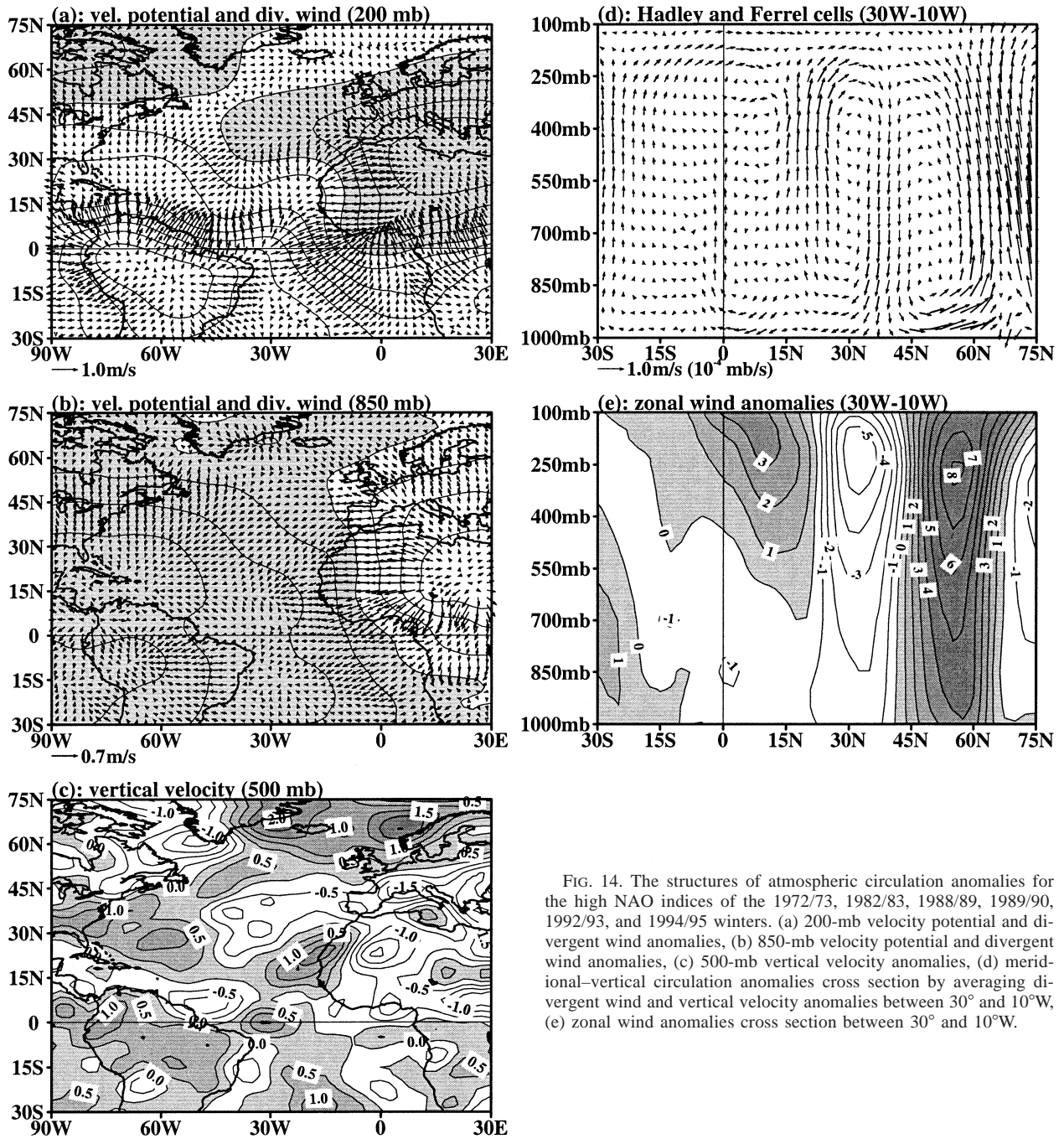


FIG. 14. The structures of atmospheric circulation anomalies for the high NAO indices of the 1972/73, 1982/83, 1988/89, 1989/90, 1992/93, and 1994/95 winters. (a) 200-mb velocity potential and divergent wind anomalies, (b) 850-mb velocity potential and divergent wind anomalies, (c) 500-mb vertical velocity anomalies, (d) meridional-vertical circulation anomalies cross section by averaging divergent wind and vertical velocity anomalies between 30° and 10°W, (e) zonal wind anomalies cross section between 30° and 10°W.

(1998) who showed a low-regression coefficient of the TSA SST anomalies with the NAO index.

The SST pattern during the high NAO index shows a tripole, with cold SST anomalies in the northwest Atlantic and in the TNA and warm SST anomalies in the mid-Atlantic. Accompanied by this SST anomaly pattern are a stronger Ferrel cell and a stronger Hadley cell. The zonal wind anomalies display westerly wind

anomalies in the North Atlantic and easterly wind anomalies in the mid-Atlantic, consistent with the strength of the Icelandic low and the Azores high during the high NAO index. The zonal wind anomaly distribution is also consistent with the meridional Ferrel and Hadley cells. The strengthening of the Ferrel and Hadley cells is associated with anomalous descending motion over the mid-Atlantic. Near the sea surface, sinking air is di-

## North Atlantic Oscillation

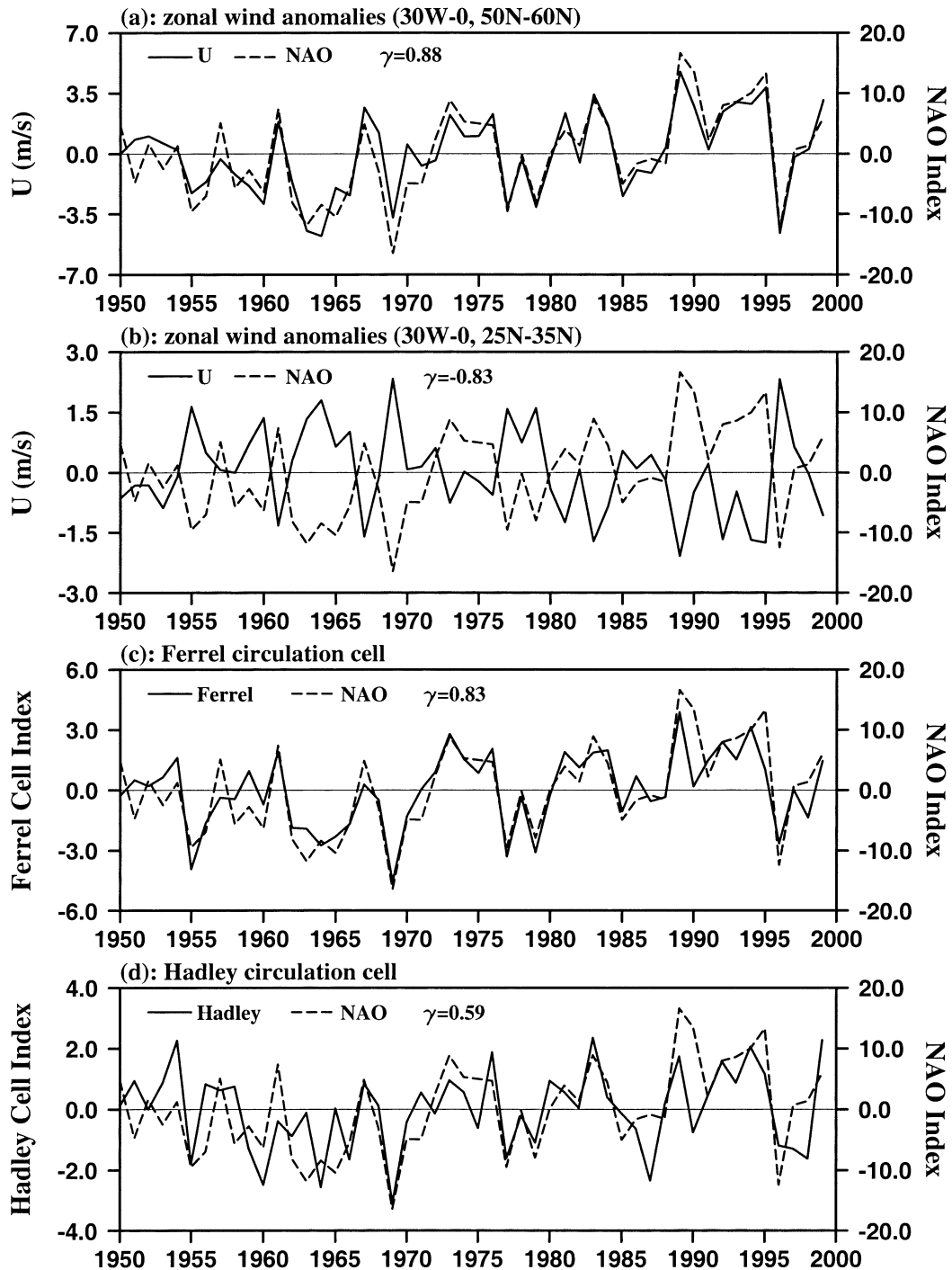


FIG. 15. Comparisons of the NAO index over the period 1950-99 with (a) 1000-mb zonal wind anomalies in the region of 50°–60°N, 30°W–0°; (b) 1000-mb zonal wind anomalies in the region of 25°–35°N, 30°W–0°; (c) the Ferrel cell index; and (d) the Hadley cell index. The Ferrel cell index is defined by 500-mb vertical velocity anomaly difference between the regions of 35°–40°N, 30°W–0° and 60°–65°N, 30°W–0°. The Hadley cell index is defined by 500-mb vertical velocity anomaly difference between the regions of 35°–40°N, 30°W–0° and 15°–20°N, 30°W–0°. All of these are calculated as winter (Dec–Mar) anomalies. The  $\gamma$  represents the correlation coefficient at zero lag.

### Relationship of NAO with Other Climate Phenomena

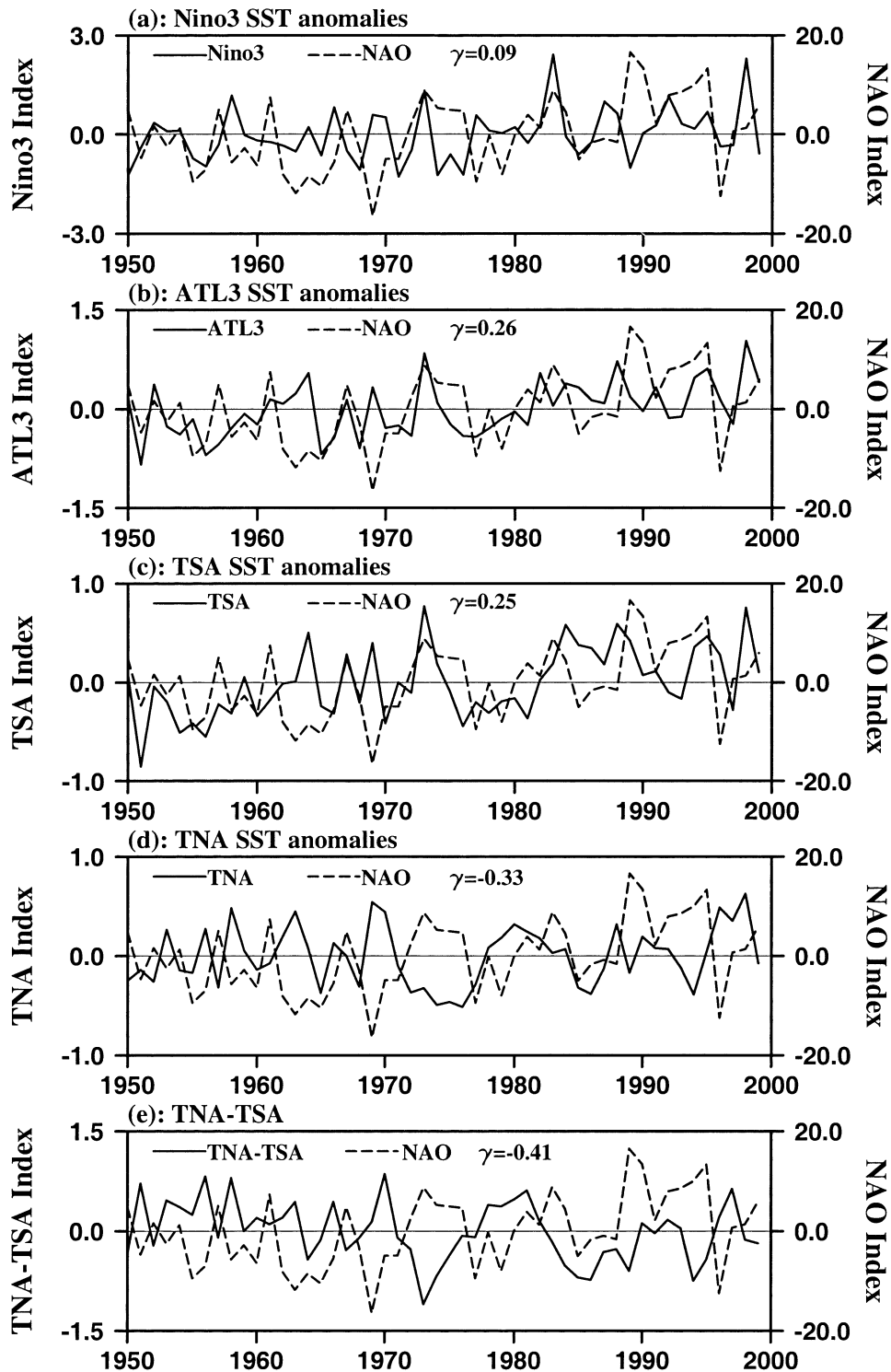


FIG. 16. Comparisons of the NAO index over the period 1950–99 with (a) the Niño-3 SST anomalies, (b) the ATL3 SST anomalies, (c) the TSA SST anomalies, (d) the TNA SST anomalies, and (e) the SST anomaly difference between the TNA and the TSA. All of these indices are calculated as winter (Dec–Mar) anomalies. The  $\gamma$  represents the correlation coefficient at zero lag.

vergent and flows both northward and southward as low branches of the Ferrel and Hadley cells, respectively. The northward (southward) flowing air is deflected to the east (west) by the Coriolis force, resulting in westerly (easterly) wind anomalies in the North (mid) Atlantic. Since the mean zonal winds are westerly in the North and mid-Atlantic (see Fig. 1), this zonal wind anomaly distribution increases (decreases) the wind speed in the North (mid) Atlantic. The increasing (decreasing) wind speed results in an increase (decrease) of latent heat flux that cools (warms) the North (mid) Atlantic. The TNA cooling during the high NAO index (Fig. 13a) is also consistent with the zonal wind anomalies in the TNA (Fig. 14e). The negative values of the surface zonal wind anomalies in the TNA indicate the strength of the northeast trade winds that will increase latent heat flux and then cool the TNA.

The Walker and Hadley circulation cells are directly driven by diabatic heating, whereas the Ferrel cell is forced mostly by transient baroclinic eddy activity through associated poleward heat and momentum transports (e.g., Holton 1992). Our analyses show that the Walker and Hadley circulations are associated with SST-related heating, consistent with the diabatic heating-driven mechanism. During the high NAO index, the North Atlantic shows cold SST anomalies, whereas the Ferrel cell is strengthened. This relationship during the high NAO index suggests that the Ferrel cell is not directly driven by SST-related heating, being consistent with the theory of the Ferrel cell.

In summary, this paper discusses Atlantic climate variability and its associated atmospheric circulation cells. The atmospheric circulation cells are identified by analyzing atmospheric divergent wind and vertical motion. The Atlantic equatorial mode involves a positive ocean-atmosphere feedback associated with the Atlantic Walker circulation, similar to the Pacific El Niño. The tropical Atlantic meridional gradient mode corresponds to an atmospheric meridional circulation cell in which the air rises over the warm SST anomaly region, flows toward the cold SST anomaly region aloft, converges in the upper troposphere to feed the strong subsidence and lower-tropospheric divergence in the cold SST anomaly region, then crosses the equator toward the warm SST region in the lower troposphere. Our analysis suggests that the Pacific El Niño can affect the TNA through the Walker and Hadley circulations, favoring the TNA warming in the subsequent spring of the Pacific El Niño year. During the high NAO index, the atmospheric meridional Ferrel and Hadley cells are strengthened, consistent with the surface westerly and easterly wind anomalies observed in the North Atlantic and in the mid-Atlantic, respectively. These winds are responsible for an alternating warm and cold SST anomaly tripole pattern observed during the high NAO index.

*Acknowledgments.* This work was supported by the National Oceanic and Atmospheric Administration

(NOAA) Office of Global Programs and by the base funding of NOAA Atlantic Oceanographic and Meteorological Laboratory. I thank D. Enfield for scientific discussions and encouragement. Comments by D. Enfield, D. Mayer, R. Molinari, J. Servain, and an anonymous reviewer help improve the manuscript. J. Harris assisted with the initial processing of the NCEP-NCAR reanalysis fields.

#### REFERENCES

- Carton, J. A., and B. Huang, 1994: Warm events in the tropical Atlantic. *J. Phys. Oceanogr.*, **24**, 888–903.
- , X. Cao, B. Giese, and A. M. Da Silva, 1996: Decadal and interannual SST variability in the tropical Atlantic Ocean. *J. Phys. Oceanogr.*, **26**, 1165–1175.
- Chang, P., L. Ji, and H. Li, 1997: A decadal climate variation in the tropical Atlantic Ocean from thermodynamic air–sea interactions. *Nature*, **385**, 516–518.
- Curtis, S., and S. Hastenrath, 1995: Forcing of anomalous sea surface temperature evolution in the tropical Atlantic during Pacific warm events. *J. Geophys. Res.*, **100**, 15 835–15 847.
- Delecluse, P., J. Servain, C. Levy, K. Arpe, and L. Bengtsson, 1994: On the connection between the 1984 Atlantic warm event and the 1982–83 ENSO. *Tellus*, **46A**, 448–464.
- Deque, M., and J. Servain, 1989: Teleconnections between tropical Atlantic sea surface temperatures and midlatitude 50 kPa heights during 1964–1986. *J. Climate*, **2**, 929–944.
- Dommenget, D., and M. Latif, 2000: Interannual to decadal variability in the tropical Atlantic. *J. Climate*, **13**, 777–792.
- Enfield, D. B., and D. A. Mayer, 1997: Tropical Atlantic sea surface temperature variability and its relation to El Niño–Southern Oscillation. *J. Geophys. Res.*, **102**, 929–945.
- , A. M. Mestas-Núñez, D. A. Mayer, and L. Cid-Serrano, 1999: How ubiquitous is the dipole relationship in tropical Atlantic sea surface temperature? *J. Geophys. Res.*, **104**, 7841–7848.
- Folland, C. K., T. N. Palmer, and D. E. Parker, 1986: Sahel rainfall and worldwide sea temperatures, 1901–85. *Nature*, **320**, 602–607.
- Hastenrath, S., 1978: On modes of tropical circulation and climate anomalies. *J. Atmos. Sci.*, **35**, 2222–2231.
- , 2000: Upper air mechanisms of the Southern Oscillation in the tropical Atlantic sector. *J. Geophys. Res.*, **105**, 14 997–15 009.
- , 2001: In search of zonal circulations in the equatorial Atlantic sector from the NCEP–NCAR reanalysis. *Int. J. Climatol.*, **21**, 37–47.
- Holton, J. R., 1992: *An Introduction to Dynamic Meteorology*. 3d ed. Academic Press, 511 pp.
- Horel, J. D., and J. M. Wallace, 1981: Planetary-scale atmospheric phenomena associated with the Southern Oscillation. *Mon. Wea. Rev.*, **109**, 813–829.
- Houghton, R. W., and Y. Tourre, 1992: Characteristics of low-frequency sea surface temperature fluctuations in the tropical Atlantic. *J. Climate*, **5**, 765–771.
- Hurrell, J. M., 1995: Decadal trends in the North Atlantic Oscillation: Regional temperature and precipitation. *Science*, **269**, 676–679.
- , 1996: Influence of variations in extratropical wintertime teleconnections on Northern Hemisphere temperature. *Geophys. Res. Lett.*, **23**, 665–668.
- Kalnay, E., and Coauthors, 1996: The NCEP/NCAR 40-Year Reanalysis Project. *Bull. Amer. Meteor. Soc.*, **77**, 437–471.
- Klein, S. A., B. J. Soden, and N. C. Lau, 1999: Remote sea surface temperature variations during ENSO: Evidence for a tropical atmospheric bridge. *J. Climate*, **12**, 917–932.
- Krishnamurti, T. N., 1971: Tropical east–west circulations during the northern summer. *J. Atmos. Sci.*, **28**, 1342–1347.
- , M. Kanamitsu, W. J. Koss, and J. D. Lee, 1973: Tropical east–west circulations during the northern winter. *J. Atmos. Sci.*, **30**, 780–787.

- Latif, M., and A. Grotzner, 2000: The equatorial Atlantic oscillation and its response to ENSO. *Climate Dyn.*, **16**, 213–218.
- Mancuso, R. L., 1967: A numerical procedure for computing fields of streamfunction and velocity potential. *J. Appl. Meteor.*, **6**, 994–1001.
- Mehta, V. M., 1998: Variability of the tropical ocean surface temperatures at decadal–multidecadal timescales. Part I: The Atlantic Ocean. *J. Climate*, **11**, 2351–2375.
- , and T. Delworth, 1995: Decadal variability of the tropical Atlantic Ocean surface temperature in shipboard measurements and in a global ocean–atmosphere model. *J. Climate*, **8**, 172–190.
- Mestas-Núñez, A. M., and D. B. Enfield, 2001: Eastern equatorial Pacific SST variability: ENSO and non-ENSO components and their climatic associations. *J. Climate*, **14**, 391–402.
- Moura, A., and J. Shukla, 1981: On the dynamics of droughts in northeast Brazil: Observations, theory, and numerical experiments with a general circulation model. *J. Atmos. Sci.*, **38**, 2653–2675.
- Neelin, J. D., D. S. Battisti, A. C. Hirst, F.-F. Jin, Y. Wakata, T. Yamagata, and S. E. Zebiak, 1998: ENSO theory. *J. Geophys. Res.*, **103**, 14 262–14 290.
- Nobre, P., and J. Shukla, 1996: Variations of sea surface temperature, wind stress, and rainfall over the tropical Atlantic and South America. *J. Climate*, **9**, 2464–2479.
- Philander, S. G., 1990: *El Niño, La Niña, and the Southern Oscillation*. Academic Press, 289 pp.
- Rajagopalan, B., Y. Kushnir, and Y. M. Tourre, 1998: Observed decadal midlatitude and tropical Atlantic climate variability. *Geophys. Res. Lett.*, **25**, 3967–3970.
- Robertson, A. W., C. R. Mechoso, and Y. J. Kim, 2000: The influence of Atlantic sea surface temperature anomalies on the North Atlantic Oscillation. *J. Climate*, **13**, 122–138.
- Rodwell, M. J., D. P. Powell, and C. K. Folland, 1999: Oceanic forcing of the wintertime North Atlantic Oscillation and European climate. *Nature*, **398**, 320–323.
- Ruiz-Barradas, A., J. A. Carton, and S. Nigam, 2000: Structure of interannual-to-decadal climate variability in the tropical Atlantic sector. *J. Climate*, **13**, 3285–3297.
- Sciremammano, F., 1979: A suggestion for the presentation of correlations and their significance levels. *J. Phys. Oceanogr.*, **9**, 1273–1276.
- Seager, R., Y. Kushnir, M. Visbeck, N. Naik, J. Miller, G. Karhmann, and H. Cullen, 2000: Causes of Atlantic Ocean climate variability between 1958 and 1998. *J. Climate*, **13**, 2845–2862.
- Servain, J., 1991: Simple climatic indices for the tropical Atlantic Ocean and some applications. *J. Geophys. Res.*, **96**, 15 137–15 146.
- , J. Picaut, and J. Merle, 1982: Evidence of remote forcing in the equatorial Atlantic Ocean. *J. Phys. Oceanogr.*, **12**, 457–463.
- , I. Wainer, J. P. McCreary, and A. Dessier, 1999: Relationship between the equatorial and meridional modes of climatic variability in the tropical Atlantic. *Geophys. Res. Lett.*, **26**, 485–488.
- , —, H. L. Ayina, and H. Roquet, 2000: The relationship between the simulated climatic variability modes of the tropical Atlantic. *Int. J. Climatol.*, **20**, 939–953.
- Smith, T. M., R. W. Reynolds, R. E. Livezey, and D. C. Stokes, 1996: Reconstruction of historical sea surface temperature using empirical orthogonal functions. *J. Climate*, **9**, 1403–1420.
- Sutton, R. T., S. P. Jewson, and D. P. Rowell, 2000: The elements of climate variability in the tropical Atlantic region. *J. Climate*, **13**, 3261–3284.
- Visbeck, M., and Coauthors, 1998: Atlantic climate variability experiment prospectus. A consensus document of U.S. and European scientists reflecting the findings of workshops in Lamont (September 1997), Dallas (February 1998), and Florence (May 1998). 49 pp.
- Wallace, J. M., and D. S. Gutzler, 1981: Teleconnections in the geopotential height field during the Northern Hemisphere winter. *Mon. Wea. Rev.*, **109**, 784–812.
- Wang, C., 2002: Atmospheric circulation cells associated with the El Niño–Southern Oscillation. *J. Climate*, **15**, 399–419.
- , and D. B. Enfield, 2001: The tropical Western Hemisphere warm pool. *Geophys. Res. Lett.*, **28**, 1635–1638.
- Weare, B. C., 1977: Empirical orthogonal analysis of Atlantic Ocean surface temperatures. *Quart. J. Roy. Meteor. Soc.*, **103**, 467–478.
- Xie, S. P., 1999: A dynamic ocean–atmosphere model of the tropical Atlantic decadal variability. *J. Climate*, **12**, 64–70.
- , and Y. Tanimoto, 1998: A pan-Atlantic decadal climate oscillation. *Geophys. Res. Lett.*, **25**, 2185–2188.
- Zebiak, S. E., 1993: Air–sea interaction in the equatorial Atlantic region. *J. Climate*, **6**, 1567–1586.